



**HAL**  
open science

# The conserved yeast protein Knr4 involved in cell wall integrity is a multi-domain intrinsically disordered protein

Manon Batista, Ellen I.M. Donker, Cécile Bon, Myriam Guillien, Adriana Caisso, Lionel Mourey, Jean-Marie François, Laurent Maveyraud, Didier Zerbib

## ► To cite this version:

Manon Batista, Ellen I.M. Donker, Cécile Bon, Myriam Guillien, Adriana Caisso, et al.. The conserved yeast protein Knr4 involved in cell wall integrity is a multi-domain intrinsically disordered protein. *Journal of Molecular Biology*, 2023, 435 (10), pp.168048. 10.1016/j.jmb.2023.168048 . hal-03874437v2

**HAL Id: hal-03874437**

**<https://hal.science/hal-03874437v2>**

Submitted on 14 Nov 2023

**HAL** is a multi-disciplinary open access archive for the deposit and dissemination of scientific research documents, whether they are published or not. The documents may come from teaching and research institutions in France or abroad, or from public or private research centers.

L'archive ouverte pluridisciplinaire **HAL**, est destinée au dépôt et à la diffusion de documents scientifiques de niveau recherche, publiés ou non, émanant des établissements d'enseignement et de recherche français ou étrangers, des laboratoires publics ou privés.



# The Conserved Yeast Protein Knr4 Involved in Cell Wall Integrity Is a Multi-domain Intrinsically Disordered Protein

Manon Batista<sup>1,2†</sup>, Ellen I. M. Donker<sup>1,2†</sup>, Cécile Bon<sup>2†</sup>, Myriam Guillien<sup>1,2</sup>, Adriana Caisso<sup>1</sup>, Lionel Mourey<sup>2</sup>, Jean-Marie François<sup>1</sup>, Laurent Maveyraud<sup>2\*</sup> and Didier Zerbib<sup>1\*</sup>

1 - Toulouse Biotechnology Institute (TBI), Université de Toulouse, CNRS, INRAE, INSA, F-31077 Toulouse, France

2 - Institut de Pharmacologie et de Biologie Structurale (IPBS), Université de Toulouse, CNRS, UPS, F-31062 Toulouse, France

Correspondence to Laurent Maveyraud and Didier Zerbib: [laurent.maveyraud@ipbs.fr](mailto:laurent.maveyraud@ipbs.fr) (L. Maveyraud), [didier.zerbib@insa-toulouse.fr](mailto:didier.zerbib@insa-toulouse.fr) (D. Zerbib) @D\_Zerbib\_DZ\_TBI  (D. Zerbib)

<https://doi.org/10.1016/j.jmb.2023.168048>

Edited by Monika Fuxreiter

## Abstract

Knr4/Smi1 proteins are specific to the fungal kingdom and their deletion in the model yeast *Saccharomyces cerevisiae* and the human pathogen *Candida albicans* results in hypersensitivity to specific antifungal agents and a wide range of parietal stresses. In *S. cerevisiae*, Knr4 is located at the crossroads of several signalling pathways, including the conserved cell wall integrity and calcineurin pathways. Knr4 interacts genetically and physically with several protein members of those pathways. Its sequence suggests that it contains large intrinsically disordered regions. Here, a combination of small-angle X-ray scattering (SAXS) and crystallographic analysis led to a comprehensive structural view of Knr4. This experimental work unambiguously showed that Knr4 comprises two large intrinsically disordered regions flanking a central globular domain whose structure has been established. The structured domain is itself interrupted by a disordered loop. Using the CRISPR/Cas9 genome editing technique, strains expressing *KNR4* genes deleted from different domains were constructed. The N-terminal domain and the loop are essential for optimal resistance to cell wall-binding stressors. The C-terminal disordered domain, on the other hand, acts as a negative regulator of this function of Knr4. The identification of molecular recognition features, the possible presence of secondary structure in these disordered domains and the functional importance of the disordered domains revealed here designate these domains as putative interacting spots with partners in either pathway. Targeting these interacting regions is a promising route to the discovery of inhibitory molecules that could increase the susceptibility of pathogens to the antifungals currently in clinical use.

© 2023 Elsevier Ltd. All rights reserved.

## Introduction

Proteins that do not have a defined 3D structure over all or part of their sequence, but nevertheless have biological activity, belong to the ubiquitous family of intrinsically disordered proteins (IDPs).<sup>1–6</sup> These proteins can have different types of disorder which can be restricted to certain regions known as

intrinsically disordered protein regions (IDPRs).<sup>2–3</sup> IDPs and IDPRs are frequently involved in crucial cellular processes such as signal transduction, gene regulation, and maintenance of homeostasis and are often implicated in human pathologies.<sup>1,7–8</sup> Their functions are mainly derived from their ability to interact with a large number of partners<sup>1</sup> through potentially different (dis)ordered structural

elements. The plasticity of IDPs and IDPRs, which can exist as ensemble of conformations, gives them structural adaptability and allows them to occupy hub positions in protein–protein interaction (PPI) networks.<sup>1,9–10</sup> One of this central protein in *Saccharomyces cerevisiae* is Knr4.

Knr4 contains large IDPRs, is considered as an important hub of the yeast interactome and is located at the crossroad of major parietal stress signalling pathways involved in stress signalling and antifungal sensitivity.<sup>11</sup> In *S. cerevisiae*, Knr4 is the representative of a conserved family of fungus-specific proteins called Knr4/Smi1.<sup>12</sup> *KNR4* was initially identified in the yeast *Hansenula mrakii* during a search for genes affecting cell wall  $\beta$ -1,3-glucan biosynthesis.<sup>13–14</sup> Deletion of *KNR4* has multiple physiological consequences: *knr4 $\Delta$*  mutants are hypersensitive to cell wall-targeting compounds such as caffeine, Congo red (CR) and calcofluor white (CFW),<sup>11,15</sup> they also show increased sensitivity to high temperatures and to antifungal agents such as caspofungin and cercosporamide.<sup>13,15–17</sup> These phenotypes appear to be correlated with changes in the cell wall composition and the concentration of chitin, to which CR and CFW bind, increases while that of  $\beta$ -glucan decreases significantly.<sup>13</sup>

Two signalling pathways play a central role in cell wall biogenesis, maintenance and stress resistance: the cell wall integrity (CWI) pathway,<sup>18</sup> and the calcineurin (CN) pathway.<sup>19</sup> In the CWI pathway, Knr4 is required for appropriate targeting of the transcription factors Rlm1p and Swi4p by the mitogen-activated protein kinase (MAPK) Slt2<sup>20</sup> involved in cell wall remodelling.<sup>18,21</sup> The link between *KNR4* and the CN pathway was supported by the sensitive phenotype to calcium stress exhibited by *knr4 $\Delta$*  mutants.<sup>22</sup> The CWI and CN pathways are not essential individually, but each becomes essential if the other is inactivated.<sup>18</sup> Similarly, the *KNR4* gene is not essential for yeast growth, but its deletion makes both pathways (CWI and CN) essential and renders the cell hypersensitive to cell wall stresses and to antifungal agents.<sup>20,23</sup> Knr4 physically interacts with the MAPK Slt2 of the CWI pathway and with the Calcineurin phosphatase Cna1 of the CN pathway.<sup>20,24</sup> This indicates that Knr4 is probably also physically at the crossroad of these two signalling pathways.

More generally, the critical role played by Knr4 on yeast physiology is highlighted by the existence of a very large number of observed genetic synthetic lethal interactions (more than 250), *i.e.* the deletion of *KNR4* is lethal when combined with the deletion of each of those numerous partners. The central position of Knr4 in the yeast interactome is also reinforced by the existence of many physical interactions (39 identified protein partners).<sup>11,20,25–30</sup> Beside members of the CWI and CN signalling pathways, Knr4's partners are involved in a variety of central cellular processes related mainly to mor-

phogenesis and stress response. Knr4 partners have functions in bud emergence, polarity development, cell secretion, transcription and ubiquitination.<sup>20,26,28–30</sup> Interestingly, *KNR4* orthologs in *C. albicans*, *SMI1* and *SMI1B*, are involved in pathogenesis and in biofilm resistance to antifungal agents.<sup>31–32</sup>

Knr4 has two experimentally-confirmed properties out of the three required for a hub protein: it is at the crossroad of essential cellular pathways and it has a plethora of partners in the yeast PPI network. The third property required for Knr4 to be a hub in PPI networks is intrinsic structural flexibility.<sup>33–34</sup> The analysis of the Knr4 sequence suggests the presence of two large disordered domains flanking a potentially structured core.<sup>11,23</sup> When produced ectopically, the structured core is capable of complementing most of the *S. cerevisiae knr4* null mutant phenotypes whereas it is no more able to physically interact with members of the CWI or the CN pathway like the MAPK Slt2 from CWI and Cna1, the catalytic subunit of calcineurin from CN. The N- and C-terminal parts seem to respectively ensure or modulate specific protein–protein interactions.<sup>11,23–24,28</sup> It is possible, but not yet demonstrated to date, that these domains are truly disordered and that PPIs are responsible for specific functions of Knr4 in maintaining parietal integrity.<sup>20,24</sup>

The main objectives of this work were first to obtain a comprehensive structural view of the Knr4 protein, which potentially carries large IDPRs that may explain its status as a hub protein in yeast. Second, we aimed to correlate this multi-domain structure with its role in the sensitivity of yeast to parietal integrity disruptors. The multi-domain organisation of Knr4, as well as the ordered or disordered nature of each domain, were previously only predicted from the sequence.<sup>23</sup> We used a combination of small-angle X-ray scattering (SAXS) and crystallographic analysis to decipher the structural organization of Knr4. In addition, using the CRISPR/Cas9 genome editing technique, we constructed strains expressing various genomic deletions of the Knr4 domains at the *KNR4* locus and analysed their sensitivity to well-known cell wall disruptors (CR and CFW) that activate the CWI pathway<sup>18</sup> and to ions such as Li<sup>+</sup>, which indicate a malfunction of the CN pathway.<sup>35–36</sup> Finally, we also tested the effect of domain deletions of Knr4 on its interactions with Slt2 to complete our previous findings on many other partners.<sup>11,20,28</sup>

This work revealed that Knr4 comprises two large IDPRs and a smaller disordered loop and their importance in maintaining cell wall integrity. The identification of molecular recognition features (MoRFs), the possible presence of secondary structure in these disordered domains, as well as the importance of the disordered domains for Knr4 in the resistance to stresses, suggested that they

might be involved in interactions with partners in either pathway such as Sit2 or Cna1 to ensure a crosstalk.

In eukaryotes, Knr4/Smi1 proteins are specific to the fungal kingdom and their deletion in the yeasts *S. cerevisiae* and *C. albicans* leads to hypersensitivity to certain antifungal agents.<sup>11,31–32</sup> Targeting Knr4 interaction regions could lead to promising compounds that could be used in combinatorial therapies to reduce the high doses of antifungal agents currently required to control human pathogenic fungi.<sup>37</sup>

## Results

### Knr4 presents an ordered core flanked by two disordered domains in solution

The solution structures of different Knr4 constructs (Figure 1) were studied using SAXS. First, SAXS data were used to determine the oligomeric state of Knr4, Knr4<sup>ΔC</sup> and Knr4<sup>ΔNΔC</sup>. In addition, the degree of disorder was investigated using Kratky analysis for these molecular species.

Knr4, Knr4<sup>ΔC</sup> and Knr4<sup>ΔNΔC</sup> are monomeric in solution. The scattered intensities of Knr4, Knr4<sup>ΔC</sup> and Knr4<sup>ΔNΔC</sup> closely follow the Guinier's law in the small-*Q* region and no evidence of aggregation is observed (Supplementary Figures 1 and 2). Because mild proteolysis was apparent for the Knr4<sup>ΔC</sup> construct, online HPLC was used to isolate an intact fragment. Data with an elution volume corresponding to the intact Knr4<sup>ΔC</sup> and a stable *R<sub>g</sub>* were merged. A concentration dependence in the small-*Q* region was observed for Knr4<sup>ΔNΔC</sup> from 5 mg mL<sup>-1</sup> and above; data at 2 mg mL<sup>-1</sup> were therefore selected for further investigation. Molecular masses deduced by

forward scattering, Rambo and Tainer analysis and from Porod volume via the SaxsMoW calculator agree with the theoretical molecular masses, and reflect a monomeric behaviour of all variants at the probed concentrations (Table 1).

Knr4 contains large intrinsically disordered domains. The normalised Kratky plot of the central Knr4<sup>ΔNΔC</sup> domain shows the characteristic behaviour of a globular domain, with a typical bell-shape having a maximum of about 1.1 near  $Q \cdot R_g = \sqrt{3}$  (Figure 2(a)). On the contrary, for a random chain, the curve would rise with increasing  $Q \cdot R_g$  to reach a nearly flat region at a value between 1.5 and 2 followed at high-*Q* values (typically  $Q > 2-3 \text{ nm}^{-1}$ ) by a further increase depending on the stiffness of the polypeptide chain.<sup>38–39</sup> Knr4<sup>ΔC</sup> shows a slight increase in disorder compared to Knr4<sup>ΔNΔC</sup> but appears relatively ordered overall. In contrast, the full length Knr4 protein clearly exhibits a disordered protein behaviour with intermediate flexibility. The normalised distribution of intramolecular distances (Figure 2(b)) shows, consistent with the Kratky plots, that Knr4<sup>ΔNΔC</sup> exhibits a bell shape characteristic of a globular domain, with a most probable intramolecular distance of  $2.3 \pm 0.05 \text{ nm}$  and a maximum dimension of  $8.0 \pm 0.2 \text{ nm}$ . Knr4<sup>ΔC</sup> and Knr4 have most likely intramolecular distances of about 2.5 nm, as reflected by bell maximum, but are much more elongated, with maximum distances of  $11.0 \pm 0.3$  and  $17.0 \pm 1.0 \text{ nm}$ , respectively, as inferred from the most extended conformation significantly present in solution. This indicates that residues 346–505 are disordered. The *R<sub>g</sub>* value, as obtained from the Guinier analysis, is for Knr4<sup>ΔNΔC</sup> of  $2.3 \pm 0.1 \text{ nm}$ . This value is similar to the expected theoretical value of  $1.9 \pm 0.3 \text{ nm}$ , and emphasizes that Knr4<sup>ΔNΔC</sup> is close to globular.

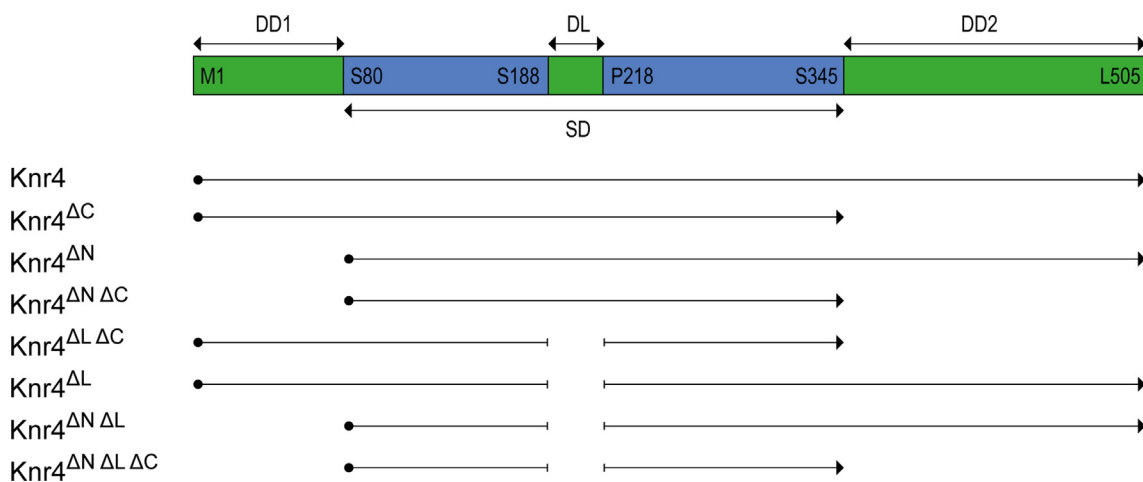


**Figure 1.** Schematic representation of the domain organisation of Knr4. Putative disordered domains (DD1, DL and DD2) are shown in green and ordered regions of SD are in blue. Residues at the domain boundaries are indicated. The different constructions used in the paper are depicted below with solid lines. N-terminus are represented by a close circle, C-terminus by an arrowhead and DL deletion boundaries by vertical bars.

Table 1 Theoretical and observed protein parameters.

Protein		Knr4 <sup>ΔC</sup>	Knr4 <sup>ΔNΔC</sup>	Knr4
<b>R<sub>g</sub> (nm)</b>	Expected <sup>1,2</sup>	2.0/5.4 ± 0.3	1.9/4.6 ± 0.3	2.3/6.5 ± 0.4
	Experimental <sup>3,4</sup>	3.2/3.2 ± 0.1	2.3/2.3 ± 0.1	4.8/5.0 ± 0.3
<b>D<sub>max</sub> (nm)</b>		11.0 ± 0.3	8.0 ± 0.2	17.0 ± 1.0
<b>Theoretical MW (kDa)</b>		39.6	30.8	57.1
<b>Experimental MW (kDa)</b>	Guinier <sup>5</sup>	39.1 ± 0.7	27.5 ± 0.5	55.0 ± 1.0
	Rambo Tainer <sup>6</sup>	38.0 ± 0.8	25.8 ± 7.1	61.3 ± 0.3
	SAXSMoW <sup>7</sup>	43.8	32.8	55.8

<sup>1,2</sup> Expected radius of gyration ( $R_g$ ) for globular proteins<sup>1</sup> or for full IDP<sup>2</sup> have been calculated respectively as described by.<sup>77,78</sup>

<sup>3,4</sup> Experimental  $R_g$  were respectively obtained from Guinier<sup>3</sup> and P(r) analysis<sup>4</sup>. Theoretical molecular weight (MW) were calculated from the primary sequences.

<sup>5,6,7</sup> Experimental MW were obtained respectively from Guinier analysis<sup>5</sup>, Rambo and Tainer concentration-independent method<sup>6</sup> and SAXSMoW calculator<sup>7,70</sup>.

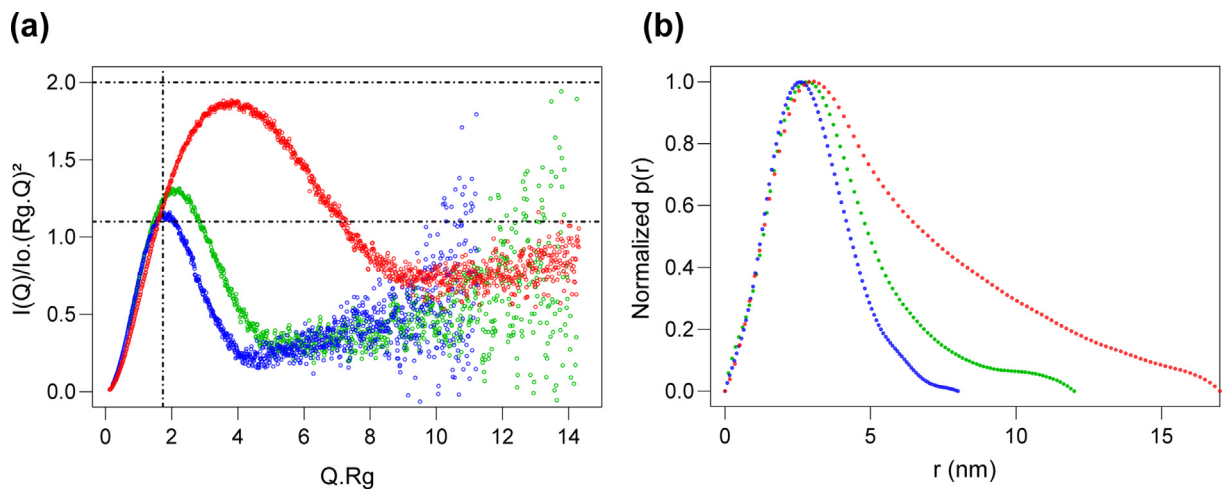


**Figure 2.** (a). Dimensionless Kratky plots of the various constructs. Knr4<sup>ΔNΔC</sup> is in blue, Knr4<sup>ΔC</sup> in green and Knr4 in red. (b). Normalized distribution of intramolecular distances.

On the contrary, the  $R_g$  values of  $3.2 \pm 0.1$  and  $4.8 \pm 0.3$  nm for Knr4<sup>ΔC</sup> and Knr4, are intermediate between that of their theoretical globular (2.0 and 2.3 nm, respectively) or IDP counterparts (5.4 and 6.5 nm, respectively) (Table 1).

### Crystallographic structures of the ordered core of Knr4

The purification of the Knr4<sup>ΔNΔC</sup>, its crystallisation and preliminary crystallographic data were described before,<sup>40</sup> but the low resolution of the data did not allow to solve the corresponding structure. Here, the core domain including or not the disordered loop DL (Knr4<sup>ΔNΔC</sup> and Knr4<sup>ΔNΔCΔC</sup>), were both purified, crystallised and both structures were solved. Crystals that belong to the hexagonal space group  $P6_2$  ( $a = b = 103.0$  Å,  $c = 93.4$  Å) with two molecules in the asymmetric unit were obtained with both constructs. The refined structure of Knr4<sup>ΔNΔC</sup> comprises residues 84–148 (residue numbering refers to mature full length Knr4), 155–

188, 218–300 and 310–347 in chain A and 84–186, 217–300 and 310–341 in chain B: a few residues are disordered at the N-terminus of both chains (7 from the N-terminus tag and residues 80 to 83) as well as at 6 residues at the C-terminus of chain B (missing residues from the tag). The structure of the ordered core of Knr4 is built of a central 6-stranded  $\beta$ -sheet (strands s1 to s6), surrounded by 7  $\alpha$ -helices (helices h1 to h7) and a small 3-stranded antiparallel  $\beta$ -sheet (strands s7 to s9) (Figure 3). The DL (residues 188–218) that connects helix h5 to strand s1 is disordered in both chains of the asymmetric unit. The final  $R$  and  $R_{free}$  factors are 0.1849 and 0.2261, respectively (Supplementary Table 1). The structure of the SD domain deleted from DL (Knr4<sup>ΔNΔCΔC</sup>) showed that this deletion does not result in significant structural modifications: residues bordering the deletion remain disordered in molecule A of the asymmetric unit of Knr4<sup>ΔNΔCΔC</sup> crystals, whereas they are defined in the electron density map of molecule B. In that molecule, deletion of DL from SD (Knr4<sup>ΔNΔC</sup>) just

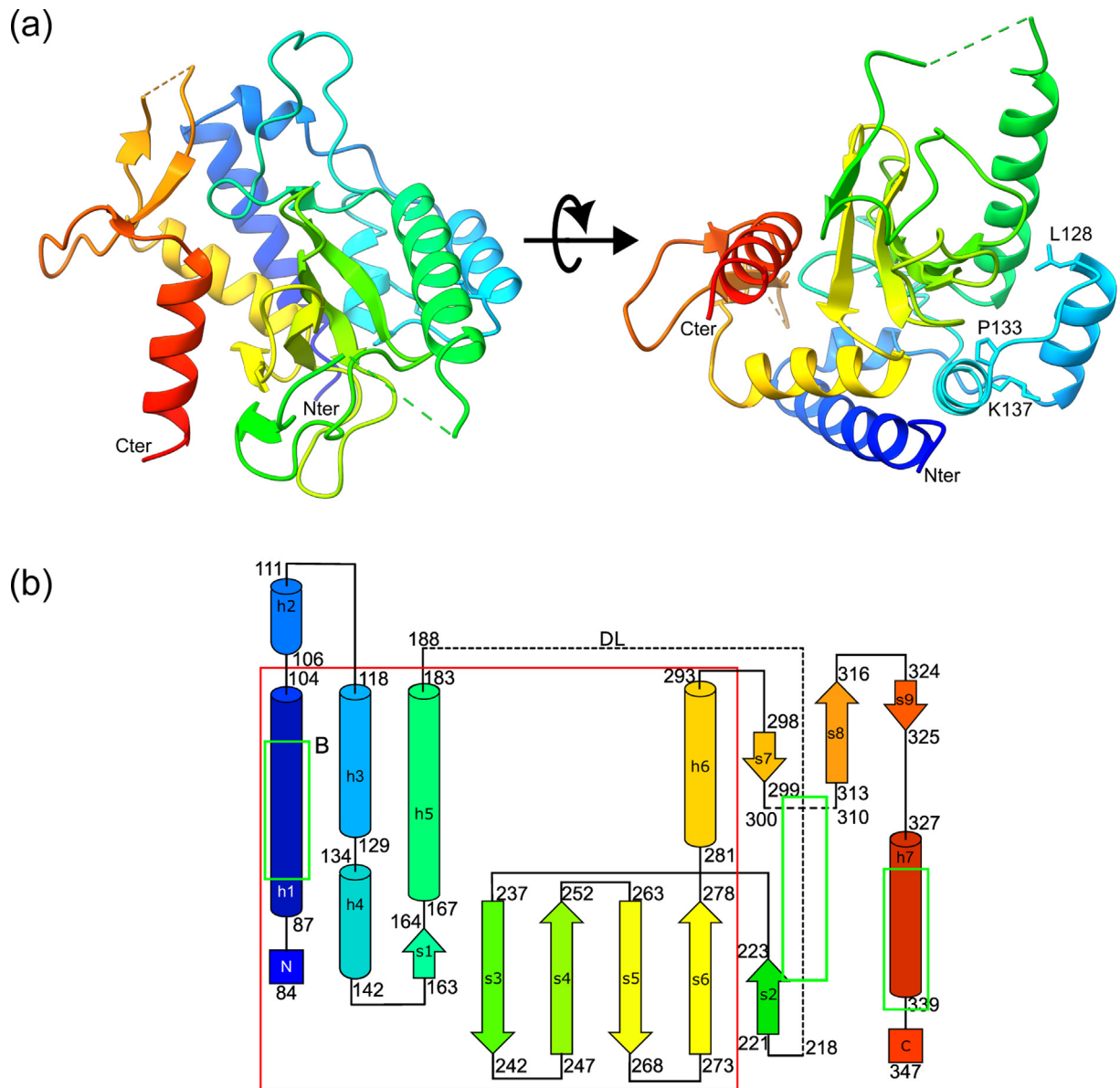


**Figure 3. (a).** Schematic representation of the structure of the ordered core of Knr4 SD. The structure is represented as a rainbow-colored ribbon, starting from blue for the N-terminal and ending in red for the C-terminal. Stretches of disordered residues with no associated electron density are represented with a discontinuous line. Conserved residues are depicted as sticks and labelled. **(b).** Topology of Knr4.  $\alpha$ -helices are symbolized with cylinders and  $\beta$ -strands with arrows. Boundaries of secondary structure elements and of disordered parts of the structure are indicated. Helices are named h1 to h7 and  $\beta$ -strands s1 to s9. Colour code is the same as in A. Red box indicates the fold common to the structure of the Smi1/Knr4-like fold. Identified MORFs are indicated with a green box.

results in a minor rearrangement at the C-terminus of helix h5 (Supplementary Figure 3).

Two molecules are found in the asymmetric unit, related by a 2-fold axis. They interact with each other through the loops connecting s2 to s3 and s4 to s5. This interface buries  $538 \pm 2 \text{ \AA}^2$  of accessible surface area of each protomer. A somewhat higher buried surface area ( $575 \pm 30 \text{ \AA}^2$ ) is found between two chains A related by crystallographic symmetry. These

potential dimerization interfaces are not predicted to be relevant for complex formation, according to PISA analysis.<sup>41</sup>

Knr4 defines a fold in the SCOP database<sup>42</sup> called the Smi1/Knr4-like fold and defined as a 3-layers  $\alpha$ - $\beta$ - $\alpha$  fold. Four structures are found with such fold: two hypothetical proteins from *Listeria innocua* (PDBID 2ICG) and *Pseudomonas syringae* (PDBID 2PAG), a putative glycan synthesis regulator from *Bacteroides fragilis* (PDBID 3D5P) and

YobK from *Bacillus subtilis* (PDBID 2PRV). This latter protein is the antitoxin component of a type II toxin-antitoxin system, and inhibits the RNase activity of YobL, its cognate toxin.<sup>43</sup> Comparison of these structures indicates that although the overall fold is similar, there are significant differences when compared to the Knr4 core structure (Figure 3). The folds of 2ICG, 2PAG, 3D5P and YobK are also made of a central 6-strand  $\beta$ -sheet, but with only 5 strands common to the  $\beta$ -sheet of Knr4: strand s2, which borders the  $\beta$ -sheet in Knr4 is lacking in the other structures (Figures 3 and 4). Also, the short helix h2 of Knr4 has no equivalent in the other structures. The 30-residues long disordered loop (residues 188–218) and strand s1 in Knr4 have no equivalent in the other structures, as the helix corresponding to helix h5 in Knr4 is directly connected to the  $\beta$ -strand corresponding to s3 of Knr4, similar to what is observed in the structure

of Knr4<sup>ANALAC</sup>. Finally, as the Knr4 core structure described herein correspond to a 263 residues long protein, whereas 2ICG, 2PAG, 3D5P, and YobK only contain 135 to 158 residues, the C-terminal part of Knr4, encompassing strands s7 to s9 and helix h7, is lacking in the other structures. Hence, the Smi1/Knr4 fold as defined in the SCOP or in PFAM databases corresponds only to a part of the Knr4 core structure presented herein, highlighted with a red frame in Figures 3 and 4.

The structure-based sequence alignment identifies only 3 strictly conserved residues: Leu128, at the C-terminal side of helix h3, and Pro133 and Lys37, at the N-terminal side and at the middle of helix h4, respectively. Leu128 and Pro133 are part of a hydrophobic cluster of residues, that also includes Phe132, Val136, Phe140, Val170, and Val171. Although these residues are not conserved in all the proteins, the

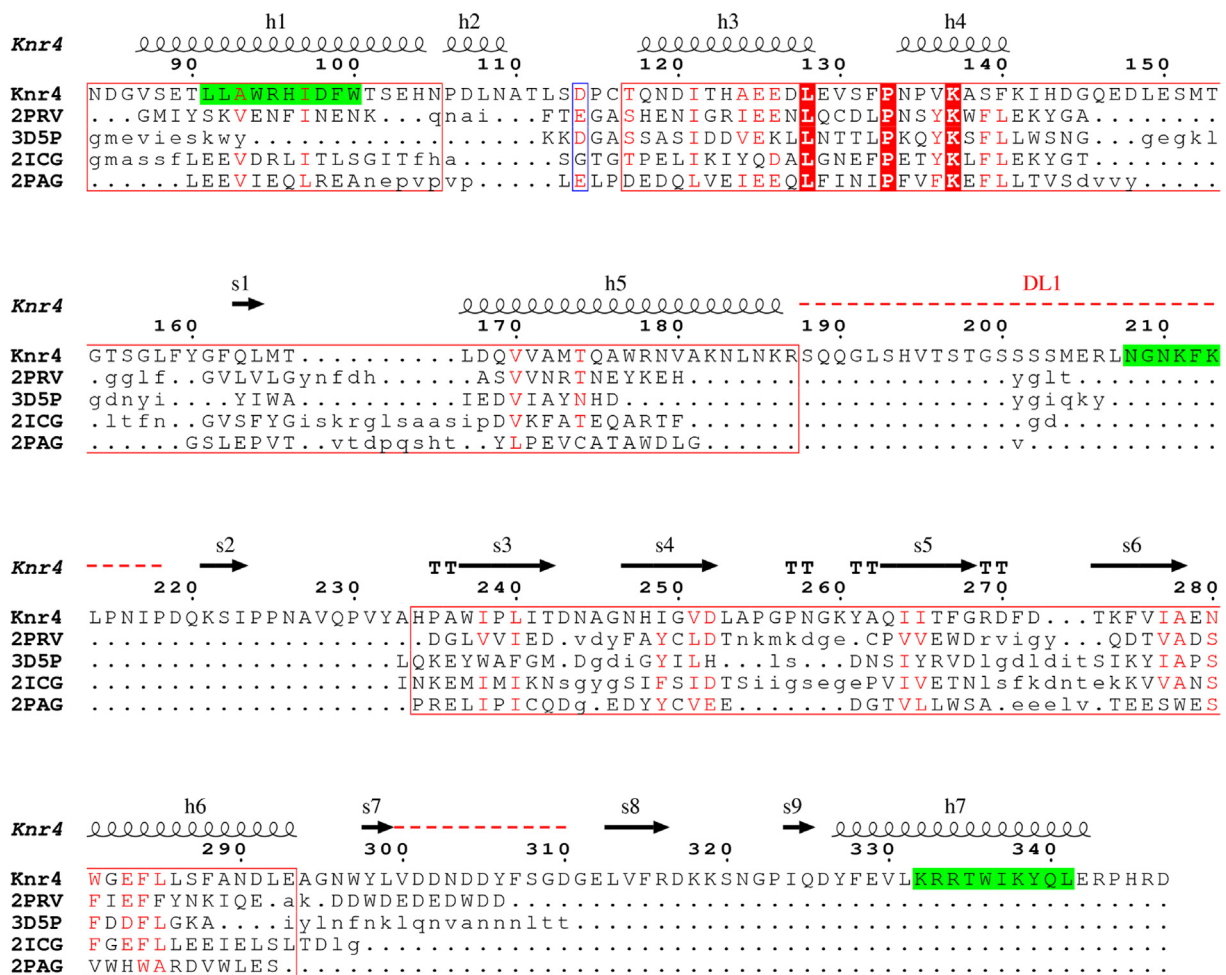


**Figure 4.** Structure-based sequence alignment of proteins identified as displaying the Smi1/Knr4 fold in the SCOP database. Knr4 secondary structure elements are displayed above the alignment. Strictly conserved residues are indicated with white letters on red background. Conserved residues are indicated in red. Lower case letters indicate regions where the structures do not align with Knr4. Disordered loops in Knr4 structures are indicated with a dashed red line in the secondary structure scheme. The red frames highlight the structurally conserved regions in the five structures. Identified MORFs are indicated with a green background.

hydrophobic cluster is found in all cases. In Knr4, the side-chain amine group of Lys137 points to the surface of the protein, at hydrogen bond distance from the side chain of Glu125 (Glu or Gln in the other structures) and Asn134.

### Comparison with crystallographic structure and flexibility modelling

The solution structures obtained from the SAXS analysis were compared with the crystallographic structure of Knr4<sup>ΔNΔC</sup>. Completed models were proposed for the Knr4, Knr4<sup>ΔC</sup> and Knr4<sup>ΔNΔC</sup> entities considering their eventual flexible regions.

The core of Knr4 has the same structure in the crystal and in solution. The A-chain was extracted from the crystallographic structure of Knr4<sup>ΔNΔC</sup> and the missing residues (80–83, 149–154, 189–217, 301–309), corresponding mainly to loops, were modelled as static residues using Allosmod-FoXS.<sup>44</sup> The best model led to excellent agreement ( $\chi = 0.761$ , compared to 2.207 without modelling the missing loops) with the corresponding experimental scattering curve (Figure 5(a)).

Modelling of the flexibility of Knr4<sup>ΔNΔC</sup>, Knr4<sup>ΔC</sup>, and Knr4 entities. The conformational states in solution of Knr4<sup>ΔNΔC</sup>, Knr4<sup>ΔC</sup>, and Knr4 were analysed using the Ensemble Optimization Method (EOM) in addition to the previous static analysis of the globular Knr4<sup>ΔNΔC</sup>. The EOM analysis of Knr4<sup>ΔNΔC</sup> provided a  $\chi$ -value of 0.679 and very good residuals (Figure 5 (a)), similar to the static analysis. The ensemble analysis revealed a tight set of discrete conformations with an overall  $R_g$  and  $D_{max}$  respectively of 2.3 and 8.6 nm and a corresponding weighted standard deviation of 0.05 and 0.7 nm (Figure 5(c) and Supplementary Table 2), in agreement with its expected static behaviour. The ensemble analysis for Knr4<sup>ΔC</sup> led to a  $\chi$ -value of 0.93 and revealed a set of discrete conformations with an overall  $R_g$  and  $D_{max}$  of 3.1 and 11.6 nm respectively and corresponding weighted standard deviation of 0.7 and 2.8 nm (Supplementary Table 2). The ensemble analysis for Knr4 led to a  $\chi$ -value of 0.88 with an overall  $R_g$  and  $D_{max}$  of 4.6 and 15.6 nm respectively and revealed greater flexibility with two broad conformational populations leading to  $R_g$  and  $D_{max}$  weighted standard deviation of 1.0 and 3.7 nm respectively. The resulting populations can be seen in Figure 5 (c) aligned via their SD domain.

### Knr4 disordered domains are required for efficient cell-wall stress resistance in yeast

To avoid expression artefacts due to ectopic production of complementation genes, CRISPR/Cas9 technology was used to construct genomic deletions of disordered domains of Knr4. A series of plasmids was constructed allowing to generate PCR fragments for allelic exchange at the *KNR4*

locus with genes encoding Knr4 protein deleted of one domain (Knr4<sup>ΔN</sup> lacking DD1, Knr4<sup>ΔL</sup> lacking DL, and Knr4<sup>ΔC</sup> lacking DD2), two domains (Knr4<sup>ΔNΔL</sup>, lacking DD1 and DL, Knr4<sup>ΔNΔC</sup> lacking DD1 and DD2, and Knr4<sup>ΔLΔC</sup> lacking DL and DD2) or all three domains (Knr4<sup>ΔNΔLΔC</sup>, lacking DD1, DL and DD2) (Figure 1). CR and CFW, known to bind growing chitin chains in the cell wall and affect its assembly,<sup>45–46</sup> were used to assess the role of each Knr4 domain in cell wall stress sensitivity.<sup>47–48</sup> The *slt2Δ* strain, deleted for the CWI pathway MAPK Slt2,<sup>49</sup> was used as a reference strain as it is hypersensitive to cell wall stressors like CR and CFW. In addition, Slt2 is known to interact with Knr4.<sup>20,28,50</sup> As expected, *slt2Δ* and the *knr4Δ* strains are hypersensitive to CR and CFW, while the wild-type strain is fully resistant in the same conditions (Figure 6). Deletion of the C-terminal domain alone does not significantly affect resistance whereas deletion of the N-terminal domain or DL increased susceptibility, even to a higher extent in the latter case (Knr4<sup>ΔL</sup>). Finally, when the deletion of the loop is combined with the deletion of either the N- (Knr4<sup>ΔNΔL</sup>), the C- (Knr4<sup>ΔLΔC</sup>) or both domains (Knr4<sup>ΔNΔLΔC</sup>), the strains were as susceptible as the *knr4Δ* and *slt2Δ* strains. In all cases, further deletion of DL results in higher susceptibility to CW stresses. More precision was obtained on the effect of each deletion by following the growth curves of these strains (Figure 6) in the presence or absence of CR or CFW. This was particularly true in the presence of CR where three phenotypic groups emerged, represented in blue, green and orange on Figure 6. The importance of the N-terminal domain and DL in stress resistance was still clearly visible, as their deletion resulted in a significantly reduced growth rate, and their combined deletion renders the strain as susceptible as the *knr4* or *slt2* null mutants. The deletion of the C-terminal domain alone does not have a visible effect on the growth rate. However, when it is deleted in addition to either the N-terminal domain or DL deletion, the growth rate is restored to normal. It therefore appears that deletion of the C-terminal domain is able to rescue the effect of the deletion of the other two. However, this deletion could not rescue the combined deletion of the N-terminal domain and DL. This suggests that the inhibitory effect of the C-terminal domain might be due to a simultaneous interaction with the N-terminal domain and DL. In the presence of CFW, a similar trend was observed but, as the effect of CFW on growth is weaker, differences in growth rate were smaller and the results were less clear.

### Knr4 disordered domains are required for LiCl resistance in yeast

Calcineurin-deficient yeasts show increased sensitivity to monovalent cations such as Na<sup>+</sup> and Li<sup>+</sup>, but not to K<sup>+</sup> or divalent cations Ca<sup>2+</sup> or Mg<sup>2+</sup>.<sup>35–36,51</sup> To test the effect of the deletion of

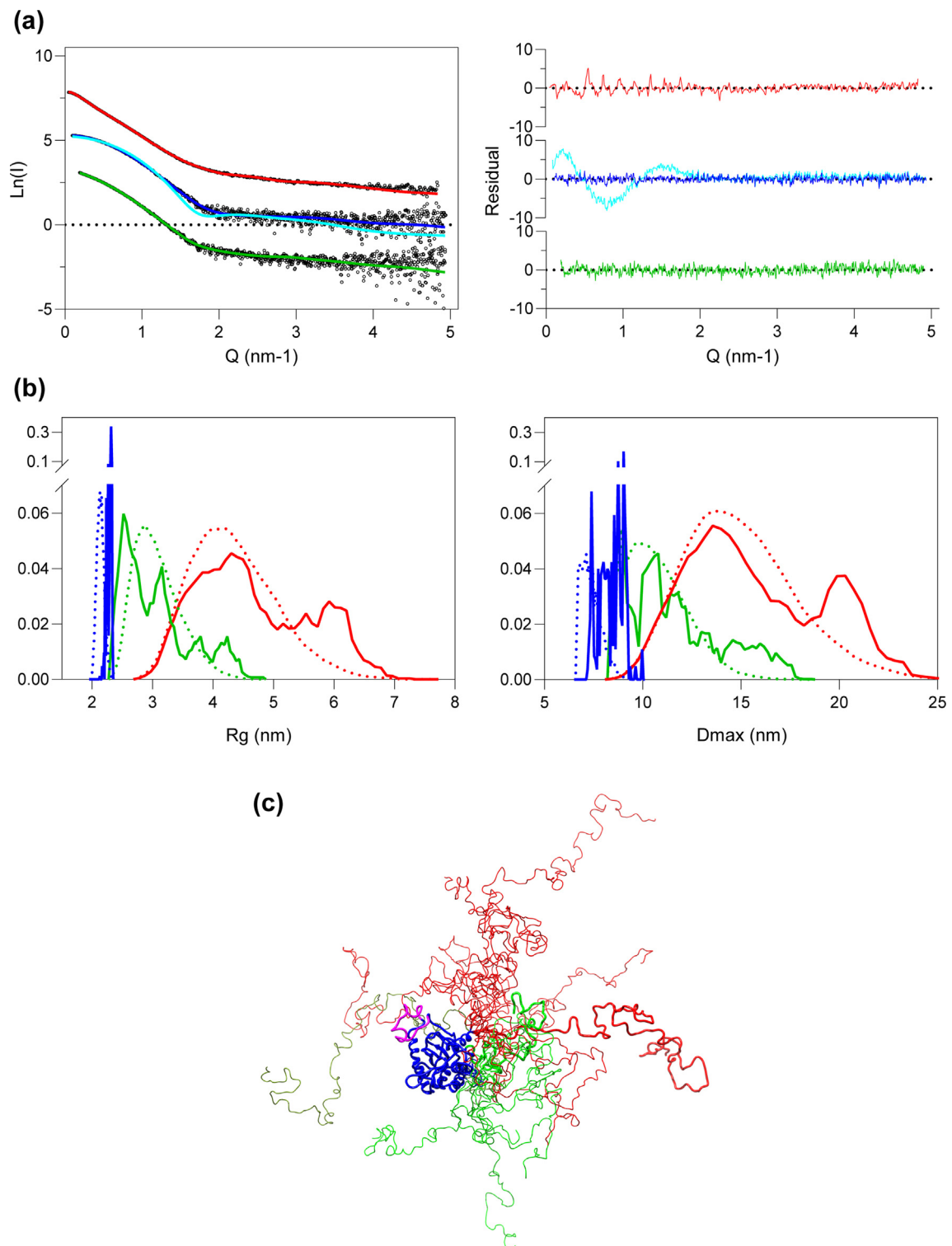


**Figure 5.** Flexibility modelling of the different entities **(a)**. Fit (left panel) and residual (right panel) obtained with corresponding experimental data (in black) for  $\text{Knr4}^{\Delta\text{C}}$  (green),  $\text{Knr4}^{\Delta\text{N}\Delta\text{C}}$  (blue) and  $\text{Knr4}$  (red). The fit and residual with the crystallographic model without modelling of the missing residues are depicted in cyan. **(b)**. Histograms of the distribution of  $R_g$  and  $D_{\text{max}}$  values of the different entities obtained respectively from the ensemble selected by EOM (solid line) and the pool (dotted line). **(c)**. The hybrid model showing the most likely conformations aligned via their SD domain with the  $\text{Knr4}^{\Delta\text{N}\Delta\text{C}}$  (SD) structure after modelling of the missing residues in blue, the N- and C-terminal domains in green and red respectively and the DL loop in magenta. The most populated conformation (21%) is represented by a thick line.

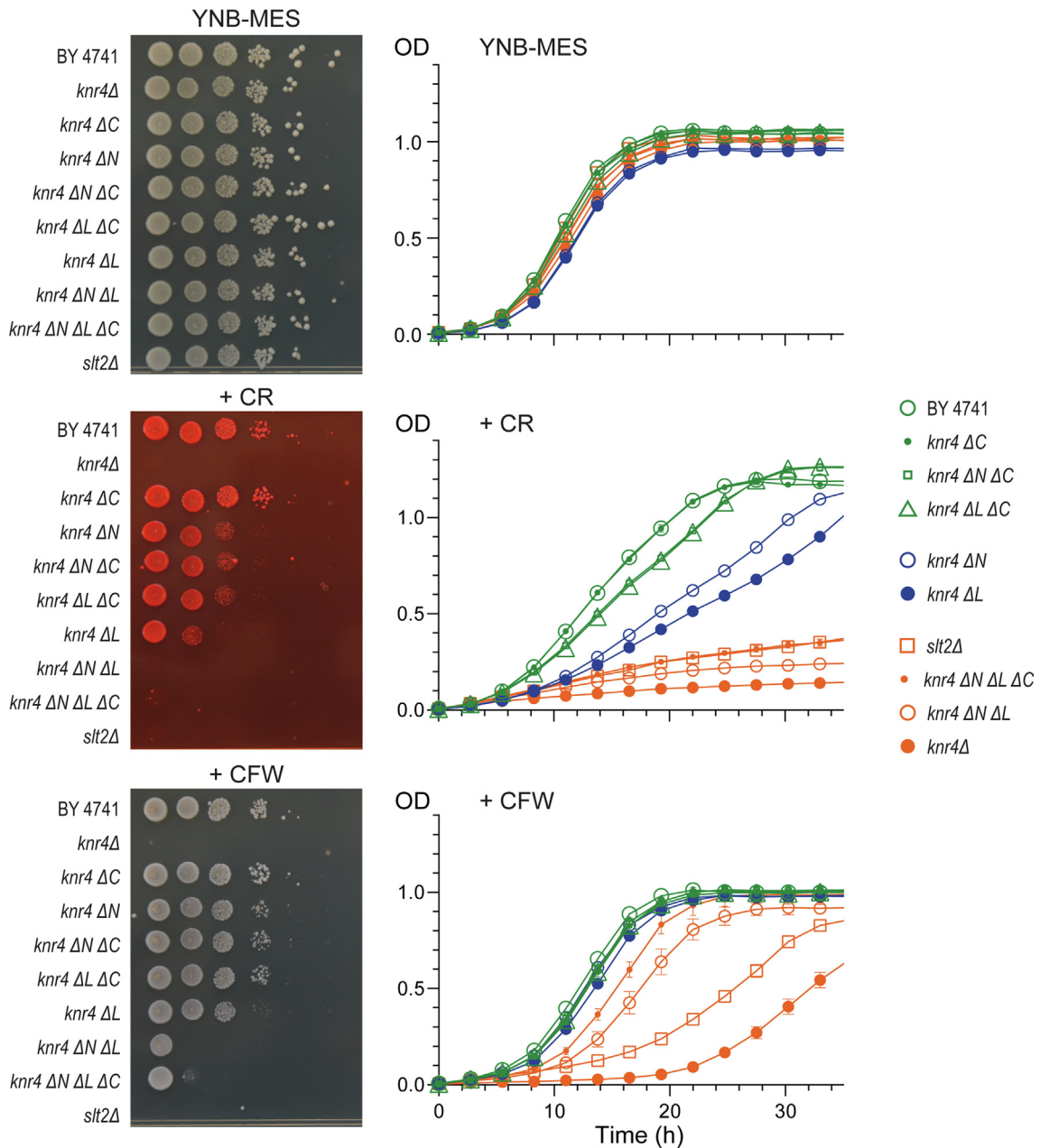


**Figure 6.** Effect of CR and CFW on growth of Knr4 mutant strains. **(Left column).** Growth on YNB-MES plates of serial dilutions (10x) of wild-type BY4741 (WT) and its isogenic deletion mutants of either a full-length gene (*knr4Δ* and *slt2Δ*) or specified domains of Knr4 (*knr4<sup>ΔC</sup>*, *knr4<sup>ΔN</sup>*, *knr4<sup>ΔL</sup>*, *knr4<sup>ΔNΔC</sup>*, *knr4<sup>ΔLΔC</sup>*, *knr4<sup>ΔNΔL</sup>* and *knr4<sup>ΔNΔLΔC</sup>*) in the presence of CR (50  $\mu\text{g}\cdot\text{mL}^{-1}$ ) or CFW (30  $\mu\text{g}\cdot\text{mL}^{-1}$ ). **(Right column).** Growth curves of wild-type BY4741 (WT) and its isogenic deletion mutants of either a full-length gene (*knr4Δ* and *slt2Δ*) or specified domains of Knr4 in absence or presence of CR (30  $\mu\text{g}\cdot\text{mL}^{-1}$ ) or CFW (30  $\mu\text{g}\cdot\text{mL}^{-1}$ ). The colour codes and symbols used to represent the growth curves are indicated.

*KNR4* or of its structural domains on the function of the CN pathway we performed the same *in vivo* experiments as above but in the presence of LiCl (Figure 7). As controls we used strains deleted of the regulatory B subunit of calcineurin (*cnb1Δ*) or of the catalytic A subunit of calcineurin (*cna1Δ*). *cnb1Δ* was fully sensitive to LiCl, as expected, while *cna1Δ* was fully resistant, as the result of the exist-

ence of *CNA2*, a redundant paralog of *CNA1*. Deletion of *KNR4* induced hypersensitivity, indicating a role for Knr4 in the CN pathway. There is no effect of single domain deletion (Knr4<sup>ΔN</sup>, Knr4<sup>ΔL</sup> or Knr4<sup>ΔC</sup>) or when deletion of the N terminus or the loop are combined with deletion of the C-terminal domain (Knr4<sup>ΔNΔC</sup> and Knr4<sup>ΔLΔC</sup>): they behave like the wild type with even a tendency to be slightly

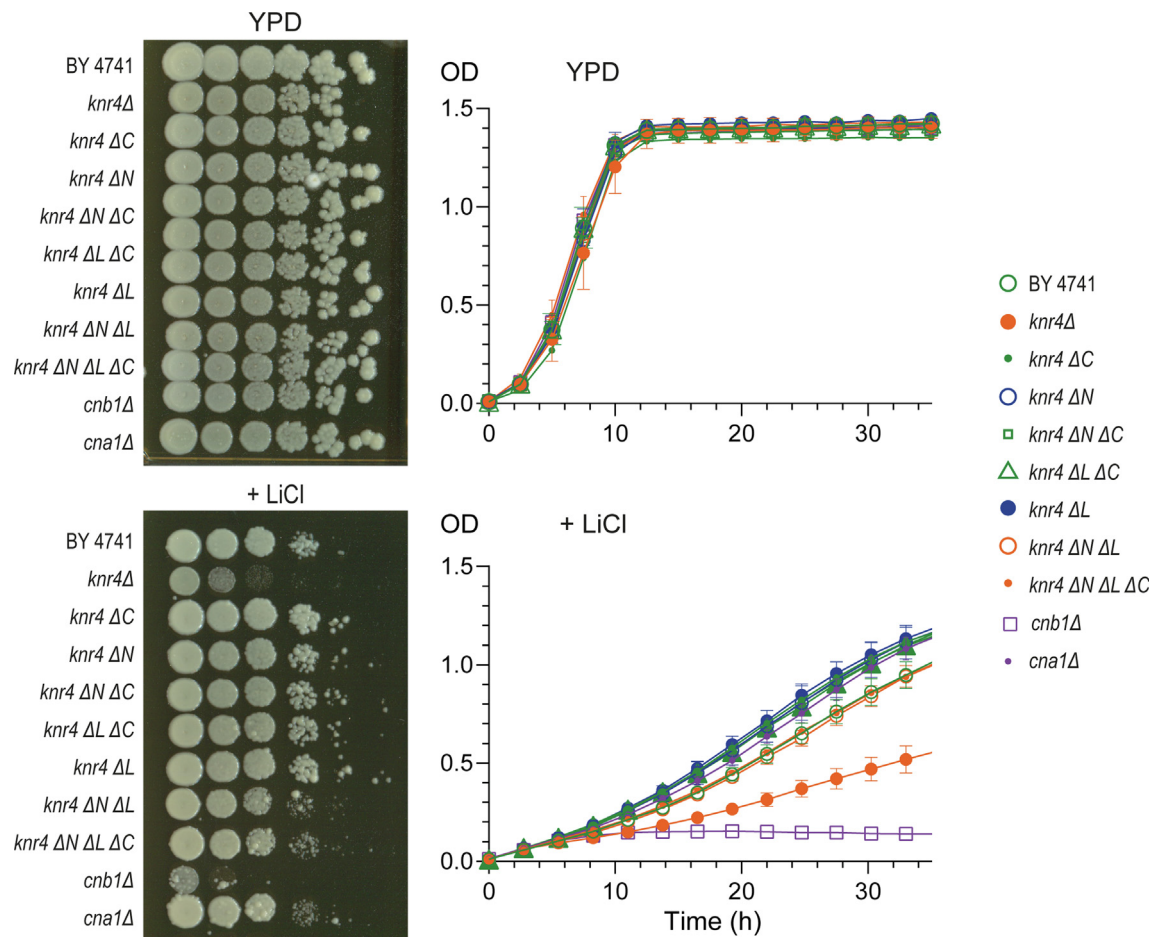


**Figure 7.** Effect of LiCl on growth of Knr4 mutant strains. **(Left column).** Growth on YPD plates of serial dilutions (10x) of wild-type BY4741 (WT) and its isogenic deletion mutants of either full-length genes (*knr4Δ*, *cnb1Δ*, *cna1Δ*) or specified domains of Knr4 (*knr4<sup>ΔC</sup>*, *knr4<sup>ΔN</sup>*, *KnR4<sup>ΔL</sup>*, *knr4<sup>ΔNΔC</sup>*, *knr4<sup>ΔLΔC</sup>*, *knr4<sup>ΔNΔL</sup>* and *knr4<sup>ΔNΔLΔC</sup>*) in the presence or not of LiCl (150 mM). **(Right column).** Growth curves of wild-type BY4741 (WT) and its isogenic deletion mutants of either a full-length gene (*knr4Δ*, *cnb1Δ*, *cna1Δ*) or specified domains of Knr4 in absence or presence of LiCl (175 mM). The colour codes and symbols used to represent the growth curves are indicated.

more resistant than the wild type. An increased sensitivity was found when both the N-terminus and the loop were deleted in the double (*KnR4<sup>ΔNΔL</sup>*) or triple (*KnR4<sup>ΔNΔLΔC</sup>*) deletion mutants suggesting that the N-terminal and loop domains are required simultaneously. No clear rescue or detrimental effect was observed when the C-terminal domain was deleted. The detrimental effect of LiCl on the wild type strain itself in liquid culture reduces the sensitivity of the growth assay (Figure 7, right panel). However, it is clear that deletion of either *CNB1* or *KNR4* greatly increased the sensitivity to LiCl. The single domain mutants (*KnR4<sup>ΔN</sup>*, *KnR4<sup>ΔL</sup>* or *KnR4<sup>ΔC</sup>*) as well as *KnR4<sup>ΔNΔC</sup>* or *KnR4<sup>ΔLΔC</sup>* tended to be more resistant to LiCl than the wild type in the drop assays, they behave similarly in liquid growth. In contrast, the *KnR4<sup>ΔNΔL</sup>*, *KnR4<sup>ΔNΔLΔC</sup>* and *cna1Δ* mutants, affected in the drop test, grew exactly like the wild type. In conclusion, as for the CWI pathway, the combined deletion of *KNR4* or of its two disordered domains

(N-terminus and DL) affects the calcineurin pathway, at least the Li<sup>+</sup> sensitivity. It indicates that Knr4 is located at a functional crossroads of the CWI and CN pathways.

#### Knr4 N- and C- disordered domains modulate the Slit2-Knr4 interaction

Knr4 was shown to interact with Slit2 in co-immunoprecipitation experiments<sup>20</sup>. In addition, yeast two-hybrid experiments (Y2H) showed that the N-terminal domain was required for the interaction of Knr4 with several partners, including Cna1 of the CN pathway.<sup>24,50,52</sup> To assess the role of these domains in the Slit2-Knr4 interaction, we performed Y2H experiments between Knr4 derivatives fused to the DNA-binding domain (BD) of Gal4 binding domain (derived from pOBD80 plasmids) and Slit2 fused to the activator domain (AD) of Gal4 (derived from pGAD-424 plasmids). A first screen was per-

formed in strain Y187 carrying a lacZ reporter gene to select the plasmid pairs inducing a positive response (Figure 8(a)). The Y187 transformants containing plasmids encoding Gal4 AD in fusion with Knr4<sup>ΔC</sup>, Knr4<sup>ΔNΔC</sup>, Knr4<sup>ΔLΔC</sup> or Knr4<sup>ΔNΔLΔC</sup>, which all lack the C-terminal domain, gave a signal above the negative controls pGAD-AgT/pGBD-Lam and the pair of empty vectors, but at a similar level than with empty pGAD-424 plasmid (Figure 8(a)). It is therefore not possible to conclude that any interaction did occur.

To find out whether these signals were indeed due to an interaction or transcriptional activation property of these Knr4 constructs, we introduced these plasmid pairs into another yeast strain (AH109) carrying 3 reporter genes (HIS3, ADE2, lacZ) and allowing a more rigorous selection by avoiding false positives. As indicated by the spot tests on selective plates (Figure 8(b)), the background observed with empty vectors was effectively eliminated by 3-AT on selective plates (-LWH + 3-AT). Two interactions were thus revealed between Slt2 and Knr4<sup>ΔC</sup> or Knr4<sup>ΔLΔC</sup>. No growth was observed on the most selective plates (-LWA) confirming that these interactions are weak. Y2H is not sensitive enough to detect the interaction of Slt2 with full size Knr4 but previous Co-IP data<sup>50</sup> and global studies<sup>28</sup> showed that this interaction exists. Here, we can conclude that deletion of the C-terminal domain greatly enhances the Knr4-Slt2 interaction and that the N-terminal region is required for the interaction to take place.

## Discussion

Earlier sequence analysis classified Knr4 in the family of proteins containing large IDPRs.<sup>2</sup> Indeed, three of the four identified structural domains were predicted as disordered: the N-terminal domain (DD1; residues 1–80), the central loop (DL; residues 185–210), and the C-terminal domain (DD2; residues 340–505).<sup>11,23</sup> SAXS data collected with Knr4, Knr4<sup>ΔC</sup>, and Knr4<sup>ΔNΔC</sup> unambiguously showed that all investigated Knr4 species were monomeric in solution and experimentally confirmed this structural organisation. The crystal structures of the ordered core of Knr4, with and without DL, were determined: the asymmetric unit of the crystal contained two interacting molecules of Knr4<sup>ΔNΔC</sup>. However, all crystal contact interfaces are predicted to be irrelevant according to PISA analysis, in agreement with our observations in solution. As IDPRs are known to be prone to proteolysis,<sup>3,53</sup> a careful attention was given to the extraction of the molecular mass in solution from the SAXS data. All three molecular species displayed molecular masses, either calculated from Guinier, concentration-independent calculation, or based on the Porod volume, in close agreement with the theoretical masses of monomeric species. This

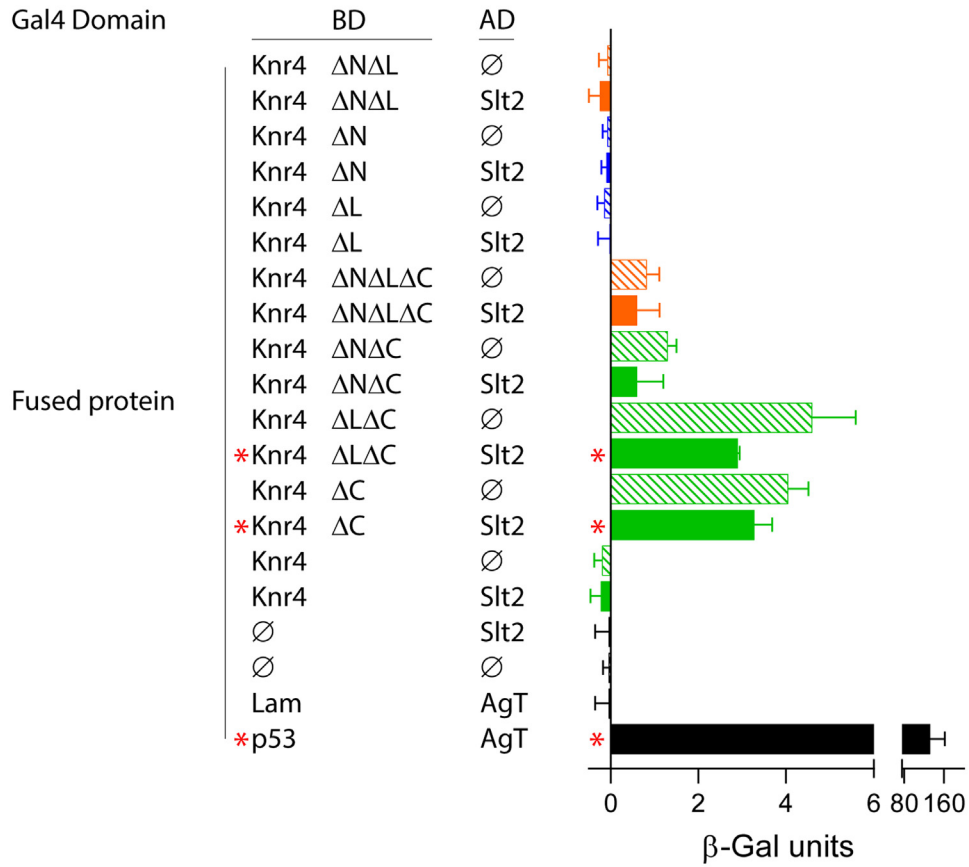
reflects that our SAXS data were collected on non-proteolyzed molecular species and rules out that the observed disorder results from degradation.

Kratky plot analysis highlights that Knr4<sup>ΔNΔC</sup> is globally well folded (with the notable exception of the DL, that encompasses 11% of the Knr4<sup>ΔNΔC</sup> construct, as this loop is missing in its crystallographic structure). Knr4<sup>ΔC</sup> is found to be slightly flexible, suggesting that the N-terminal domain DD1 is only partially unfolded, whereas the full-length Knr4 is by far the most flexible entity, highlighting the higher disorder content of the C-terminal domain DD2. These observations agree with a previous circular dichroism study,<sup>23</sup> which indicated that the C-terminal domain DD2 lacked any secondary structure in all evaluated constructions, while the N-terminal domain DD1 displayed some helical content only when the C-terminal domain was deleted. In the full-length protein, DD1 was also devoid of any structuration: the presence of the C-terminal domain DD2 seems to prevent secondary structure formation in the N-terminal domain DD1.

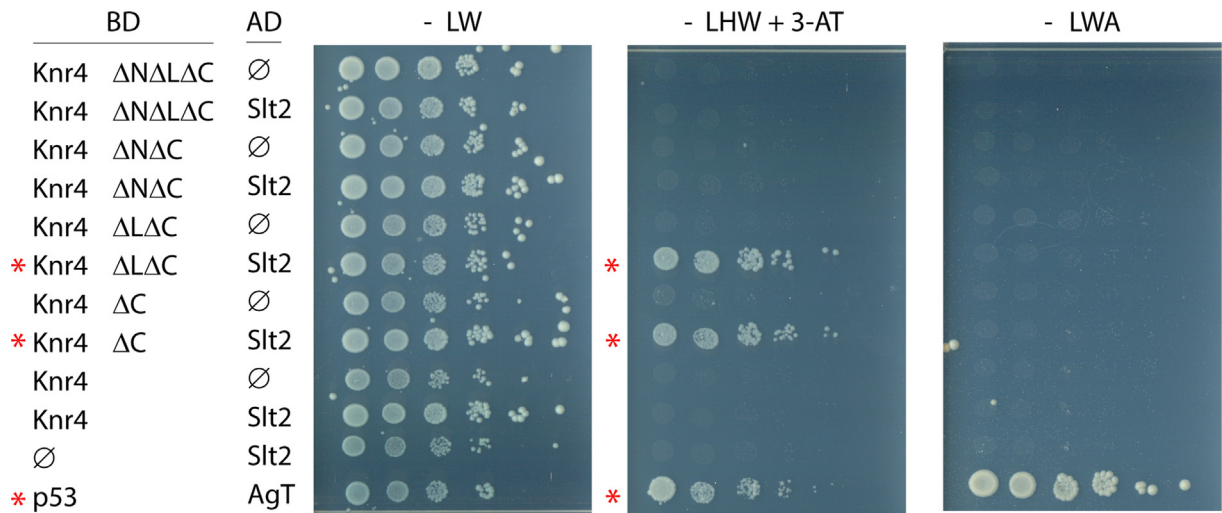
The crystallographic structure of Knr4<sup>ΔNΔC</sup> suggests that some loops are disordered in the SD domain. While residues 149–154 are only disordered in chain A of the asymmetric unit, residues 185–216 and 301–309 are disordered in both molecules of the asymmetric unit. Residues 188–218 correspond to the DL, which was identified as potentially disordered according to sequence analysis.<sup>11,23</sup> The deletion of residues 189–217, which include DL, does not significantly alter the structure of the ordered part of SD, as shown with the crystal structure of Knr4<sup>ΔNΔLΔC</sup>.

It is quite common that IDPRs/IDPRs are only partially unstructured (and not complete random coils) and contain regions of pre-structured motifs or PreSMOs, which may serve as targets for their interaction partners.<sup>54</sup> The potential presence of  $\alpha$ -helices in the N-terminal domain DD1 of Knr4, as evidenced by CD data,<sup>23</sup> could be of importance for its hub function as it has been observed previously that 62% of the protein-protein interactions are mediated by  $\alpha$ -helical structures at the interface<sup>55</sup>. Search for MoRFs within Knr4<sup>34</sup> pointed to five regions: one in the N-terminal DD1 domain (residues 5–10), three in the SD core (residues 91–100, 208–213 and 332–341) and one in the C-terminal DD2 region (residues 497–505) (Figures 3 and 4). When projected on the structure of the Knr4<sup>ΔNΔC</sup>, it appears that residues 91–100 build the central part of helix h1, residues 208–213 are part of the DL loop, and residues 332–441 build the C-terminal part of helix h7. These 3 regions are localized at the surface of the structure of Knr4<sup>ΔNΔC</sup>, and only h1 is present in the Smi1/Knr4 fold as defined in SCOP/PFAM (Figure 4). Indeed, the DL loop and helix h7 are only found in Knr4. Hence, two of these MoRFs could promote interactions specific to Knr4. According to our *in vivo* data,

(a)



(b)



the N-terminal domain DD1 and the loop DL are important for the biological function of Knr4 in both the CWI and the calcineurin pathways, which is not the case for the C-terminal domain DD2. Indeed, the single deletion of DD1 or DL results in an increased sensitivity to CR and CFW and a slower growth, and their simultaneous deletion results in the same phenotype as the  $\Delta knr4$  mutant in the presence of cell wall stressors, and in an increased sensitivity to the CN inducer LiCl. On the opposite, single deletion of the C-terminal domain DD2 does not alter the phenotype nor the growth in any case. Our data even suggests that deletion of the C-terminal domain DD2 might partly compensate the effect on CWI of DL deletion: sensitivity is lower and growth is faster for  $knr4^{\Delta DD2}$  than for  $knr4^{\Delta DL}$ . This is particularly clear when growth in the presence of CR was analysed: the combined deletion of either DL or the N-terminal domain DD1 with the C-terminal domain DD2 did not affect growth, whereas individual deletions of DL or the N-terminal domain DD1 caused a clear decrease in growth rate. This suggests that the C-terminal domain DD2 might act as a negative regulator of the function of Knr4. In that respect, CD data obtained previously by Durand and colleagues<sup>23</sup> are particularly interesting as they suggest that the presence of the C-terminal domain DD2 decreases the secondary structure content of the N-terminal domain DD1, which might result in decreased interactions with partners.

Early evidence identified members of the CWI and CN pathways as partners of Knr4,<sup>28</sup> including Cnb1, the regulatory subunit of calcineurin. In addition, the role of specific Knr4 domains was revealed for some partners, such as Tys1, the tRNA-tyrosyl synthase,<sup>24</sup> Bck2, involved like Slt2 in pKC1 signalling<sup>50</sup> and Cna1, the catalytic subunit A of calcineurin.<sup>52</sup> The N-terminal DD1 region of Knr4 as well as the central SD domain were required for these interactions and the C-terminal DD2 part was inhibitory. For Slt2, known to interact weakly with Knr4,<sup>20</sup> we have shown here that the N-terminal disordered DD1 domain of Knr4 was required whereas the C-terminal DD2 domain was inhibitory. The positive role of the N-terminal disordered domain DD1 and the loop DL and the nega-

tive role of the C-terminal domain DD2 in both the function and direct interaction of Knr4 with its partners in the CWI and CN pathways attest to its role at the crossroads of these pathways. This also suggests the existence of intramolecular interactions between these disordered regions of the protein that could also modulate intermolecular interactions with partners. Our hypothesis is that structural changes are required *in vivo* in order for such inter-domain interaction to modulate interactions with partner. The inherent flexibility of Knr4 renders this possible but an unidentified signal might initiate those structural changes. We postulate that phosphorylation could dictate the key function of Knr4 in cell wall stress signalling by modulating the folding of disordered domains before or upon binding to their partners. This would allow a switch between an open (extended) state and a closed state in which DD2 could interfere with the DD1 and/or DL interaction domains of the protein to inhibit intermolecular interactions. It has already been shown that phosphorylation can act as a regulator of IDP folding and represent a “structural switch”.<sup>56</sup> It has a major role in the competition of the 4E-binding protein 2 (4EBP2) with the eukaryotic translation initiation factor 4G (eIF4G) for binding to the initiation factor 4E (eIF4E) to prevent cap-dependent translation initiation.<sup>56–57</sup> Such a structural effect of disordered domain phosphorylation has also been observed in the interaction of Arrestins with G protein-coupled receptors to stop G protein activation and initiate key signalling.<sup>58–59</sup> Knr4 is known to be phosphorylated *in vivo* and phosphorylation sites are present in both the DL loop and the C-terminal DD2 region.<sup>11</sup> In particular, two residues of the loop, serine 200 and 203, have been shown to play a role in certain Knr4 phenotypes.<sup>23</sup> We believe that it will be very interesting to evaluate whether this phosphorylation can play a role in the structuring of Knr4 domains and notably in intramolecular interactions and the promotion or inhibition of intermolecular interactions.

Disordered domains in numerous IDPs have been found to interact with multiple partners.<sup>10</sup> The N-terminus of Knr4 becomes vital when the CWI or the CN pathway are disrupted,<sup>20</sup> and the lack of DD1 prevents interactions with Slt2 and

**Figure 8.** Y2H analysis of Knr4-Slt2 interactions. Proteins expressed in Y2H receptor strains as fusions with either the DNA binding domain of Gal4 (BD) in pOBD80 derivatives or the activation domain of Gal4 (AD) in pGAD-424 derivatives are indicated. Positive (pGBD-p53/pGAD-AgT) and negative (pGBD-p53/pGAD-Lam) controls are also indicated. Empty vectors are marked by  $\emptyset$ . (a). Screening in strain Y187.  $\beta$ -galactosidase activity was measured in the indicated transformants and expressed in  $\beta$ -Gal units as defined in the Materials and Methods section and normalized with control acellular reactions (blank). The color code used on the graph is that used in Figures 6 and 7. The hatched bars are used for transformants containing one or two empty vectors. The error bars represent the standard deviation of three to five independent titrations. (b). Y2H analysis in strain AH109. Positive plasmid pairs “selected” in the Y187 screen were introduced into the AH109 reporter strain. 10x serial dilutions of the cultures were spotted on selective plates (minus leucine and tryptophan (-LW); minus leucine, tryptophan, histidine and plus 3-AT (-LWH + 3-AT) or minus leucine, tryptophan and adenine (-LWA)). The labelling of the constructs is as in (a). The red asterisks in (a) and (b) identify the final positive interactions.

Cna1.<sup>23</sup> It is reasonable to assume that Knr4 interacts also with a lot of other proteins through these domains. The identification of MoRFs in DD1 and DL, as well as secondary structure elements in DD1, particularly in the absence of DD2, support this theory. Knr4/Smi1 proteins are specific to fungi and their absence in *S. cerevisiae* and *C. albicans* causes increased sensitivity to certain antifungal agents.<sup>11,31–32</sup> Combining Knr4 inhibitors with existing antifungal agents could reduce the high doses currently required to kill pathogenic fungi.<sup>37</sup>

## Materials and Methods

### Strains and plasmids

Plasmid constructions were performed in MC1061 recA (*E. coli* K12; F<sup>-</sup> araD139  $\Delta$ (ara-leu) 7696 galE15 galK16 recA1  $\Delta$ (lac)X74 rpsL (Str<sup>R</sup>) hsdR2 ( $r_{\text{K}}$   $m_{\text{K}}^+$ ) mcrA mcrB1) using classical cloning procedures and as recommended by enzymes and product manufacturers (Fermentas, Promega, NE Biolabs). Culture media (Lennox-Broth) were supplemented with ampicillin (150  $\mu$ g/mL) and agar when needed. The genes encoding full length Knr4 (Knr4<sup>1-505</sup>), Knr4 <sup>$\Delta$ N $\Delta$ C</sup> (Knr4<sup>80-340</sup>) and Knr4 <sup>$\Delta$ C</sup> (Knr4<sup>1-345</sup>) were cloned into pGEX-6P-3 vector (GE Healthcare), in C-terminal fusion of a cleavable (PreScission<sup>TM</sup> protease (GE Healthcare)) glutathione S-transferase (GST). Plasmids pGEX-6P-3::Knr4 and pGEX-6P-3::Knr4 <sup>$\Delta$ N $\Delta$ C</sup> have been described.<sup>23,40</sup> Plasmid pGEX-6P-3::Knr4 <sup>$\Delta$ C</sup> was constructed by introducing two in frame stop codons at codons 346 and 347 of *KNR4* in pGEX-6P-3::Knr4 by mutagenesis using self-complementary PCR primers (*KNR4*-Mut-Top and -Bot; [Supplementary Table 3](#)). Vector pGEX-6P-3::Knr4 <sup>$\Delta$ N $\Delta$ L $\Delta$ C</sup> was constructed by inverse PCR on pGEX-6P-3 using pGEX-6P-3::Knr4 as matrix and primers allowing the precise deletion of DL ( $\Delta$ L-Fwd and -Rev; [Supplementary Table 3](#)). In order to generate the repair fragments used in the CRISPR/Cas9 genome editing experiments, a genomic fragment from the *KNR4* locus of yeast BY4741 (MATa *his3 $\Delta$ 1 leu2 $\Delta$ 0 met15 $\Delta$ 0 ura3 $\Delta$ 0*) where *KNR4* is flanked by 1096 bp of upstream DNA (promoter) and 341 bp of downstream DNA (terminator) was amplified with specific primers (*KNR4*-Fwd and -Rev; [Supplementary Table 3](#)) and then cloned into an intermediate vector (pZE13-MCS, Expressys) between its BamHI and XbaI sites. This vector, pZE13::Pro-*KNR4*-Ter, was then used as a template to generate all Knr4 domain deletions shown in [Figure 1](#) by reverse PCR using specific primers ( $\Delta$ N-Fwd and -Rev,  $\Delta$ L-Fwd and -Rev and  $\Delta$ C-Fwd and -Rev; [Supplementary Table 3](#)). Derivatives of the plasmid pOBD80, (*TRP1*),<sup>60</sup> expressing the DNA-binding domain of Gal4 in fusion with either Knr4, Knr4 <sup>$\Delta$ C</sup>, Knr4 <sup>$\Delta$ N</sup> or Knr4 <sup>$\Delta$ N $\Delta$ C</sup> have been described previously<sup>11,20,28</sup> and used here as template to generate further deletions of the DL loop using specific pairs

of phosphorylated primers ([Supplementary Table 3](#)) allowing the construction of Gal4 fusions with Knr4 <sup>$\Delta$ L</sup>, Knr4 <sup>$\Delta$ L $\Delta$ C</sup>, Knr4 <sup>$\Delta$ N $\Delta$ L</sup> and Knr4 <sup>$\Delta$ N $\Delta$ L $\Delta$ C</sup>. The bait plasmid pGAD424 (*LEU2*)<sup>61</sup> encoding the activation domain of Gal4 in fusion with Sit2, pGAD424::Sit2 has been described.<sup>11,20,28</sup>

### Yeast strain construction by CRISPR/Cas9 genome editing

The yeast strain used as target was BY4741 *knr4 $\Delta$* ::KanMX4 from the YKO MATa Strain Collection (Open Biosystem). The guide RNA targeting the KanMX4 cassette as well as the Cas9 protein was provided by the plasmid pGZ110::gKan, a derivative of pML107 (Addgene) generously provided by Bruce Futcher (Stony Brook School of Medicine). This *E. coli*/yeast shuttle plasmid carries the LEU2 gene as a selection marker in yeast. The repair fragments were obtained by amplification of pZE13::Pro-*KNR4*-Ter derived vectors each carrying one or more domain deletions ([Figure 1](#)). BY4741 *knr4 $\Delta$* ::KanMX4 cells were harvested at early exponential growth (OD<sub>600nm</sub> between 0.3–0.6), washed (Lithium acetate 100 mM in TE buffer) and then concentrated (10<sup>7</sup> cells in 40  $\mu$ L) in the same buffer. These cells were transformed in a mixture containing 250 ng of pGZ110::gKan and 1  $\mu$ g of repair fragment in the presence of 25  $\mu$ g of carrier DNA (Salmon sperm ssDNA-Sigma) and 50% PEG(8000)/LiAc/TE to make up a total volume of 215  $\mu$ L. After 30 minutes incubation at 30 °C, 13  $\mu$ L of DMSO (NEB, B0515) were added. After a 10-minutes heat shock at 42 °C, cells were washed three times with 1 mL of YPD medium and incubated again for 10 minutes at 30 °C. The cells were then centrifuged, resuspended in 150  $\mu$ L of YPD and plated on YNB-Leu selective plates. The plates were incubated for 48 hours at 30 °C and the colonies were transferred to YPD plates. The *KNR4* locus was then amplified for verification by sequencing of each deletion (Eurofins).

### Yeast drop dilution growth assay

To perform growth assays on solid media, cell cultures were grown in YPD medium up to an OD<sub>600</sub> between 0.8 and 1.0 and then adjusted to an OD<sub>600</sub> of 0.9 in YPD. Tenfold serial dilutions were prepared and spotted onto YNB-CSM or YPD agar plates to evaluate their sensitivity to cell wall stress agents or LiCl. When indicated, YNB-CSM medium was supplemented with 50 mM 2-(N-Morpholino) ethane sulfonic acid (MES) buffered to pH 6. Where indicated, YNB-CSM plates were supplemented with either Congo red (Sigma-Aldrich), calcofluor white (ICN Biomedicals), and YPD plates were supplemented with 275 mM LiCl (Sigma-Aldrich). Plates were

incubated for 72 h to 96 h at 30 °C. Each assay was performed at least in triplicate.

### Saccharomyces cerevisiae microplate growth assay

Stock solutions of CR (SIGMA, PCode 102075330, 86.2% purified; 5 mg mL<sup>-1</sup> in water) and CFW (ICN Biomedicals, cat.158067, 4 mg mL<sup>-1</sup> in water clarified with 10 N sodium hydroxide) were diluted in YNB/MES to obtain concentrated 10X solutions (300 µg.mL<sup>-1</sup> and 100 µg.mL<sup>-1</sup> respectively). Overnight cultures of the tested strains (in triplicates) were collected at OD<sub>600</sub> ranging from 0.9 to 2.5, centrifuged and resuspended in YNB/MES at a theoretical OD<sub>600</sub> of 0.05 (OD<sub>600</sub> = 1 corresponds to 1.4 10<sup>7</sup> cells/mL). 20 µL of stressor or LiCl was added to 180 µL of cells and growth was monitored in 96-well plates in a microplate reader (Epoch2-Biotech) under continuous slow orbital shaking. The turbidity of the cultures was measured at 600 nm every 15 minutes for 60 hours. It should be noted that it was not possible to test higher concentrations of CR than 50 µg.mL<sup>-1</sup> as its precipitation prevented the reading. Data analysis was performed using GraphPad software (Prism 8.3.0). Triplicates were averaged and baselines (cell-free medium) were subtracted to obtain corrected growth curves. The maximum growth rate (µ max) was calculated by first transforming the baseline corrected data with  $y = \ln(y)$ . This new data was then plotted and a non-linear regression (line through the point (X0, y0)) was added to the linear region of the plotted graph. X0 and Y0 are set to “no constraints” and a linear region of the plotted graph was chosen visually. This region thus varies from strain to strain. The maximum growth rate (µ max) is the slope of this linear region.

### Yeast two-hybrid

A first screen for positive interaction was performed in the Y187 recipient strain carrying a lacZ reporter gene under the control of a Gal1 promoter (Y187: MAT $\alpha$ , ura3-52, his3-200, ade2-101, trp1-901, leu2-3, 112, gal4 $\Delta$ , met-2, gal80 $\Delta$ , URA3::GAL1<sub>UAS</sub>-GAL1<sub>TATA</sub>-lacZ; Clontech). This strain was co-transformed with derivatives of pOBD80 (*TRP1*)<sup>60</sup> expressing the Gal4 DNA binding domain in fusion with Knr4 constructs and a derivative of pGAD424 (*LEU2*)<sup>61</sup> encoding the Gal4 activation domain in fusion with the selected bait Slt2. The positive control was the pGAD-AgT/pGBD-P53 pair (Matchmaker III Clontech) giving strong  $\beta$ -galactosidase activity, the negative controls were the pGAD-AgT/pGBD-Lamin pair (Matchmaker III Clontech) and the empty vector pairs (pGAD-424/pOBD80). Transformants were first selected on YNB-CSM agar plates lacking leucine and tryptophan (-LW) and interaction positive pairs

were screened using a simple  $\beta$ -galactosidase qualitative assay performed directly on the cultures (Yeast  $\beta$ -Galactosidase assay kit, Thermo).  $\beta$ -Galactosidase activity was evaluated on cell cultures by measuring the production of ortho-nitrophenol (ONP) formed by hydrolysis of ortho-nitrophenyl- $\beta$ -galactoside (ONPG) with the following equation:  $\beta$ -Gal Unit =  $(1000 \times A_{420}) / (t \times V \times O_{D_{600}})$ . Where A420 is the difference of the absorbance (420 nm) of the tested strain minus the blank, t is the time of incubation in minutes, V is the cell volume (mL) and OD<sub>600</sub> the optical density of the cell suspension tested.

After this first screening, the positive pairs of plasmids were further introduced in another strain (AH109: MAT $\alpha$ , trp1-901, leu2-3, 112, ura3-52, his3-200, gal4 $\Delta$ , gal80 $\Delta$ , LYS2::GAL1-HIS3, MEL1 GAL2-ADE2, URA3::MEL1-lacZ, Clontech) allowing a finer selection of interactions. AH109 carries three reporter genes (*HIS3*, *ADE2* and *lacZ*) under the control of Gal4-dependent promoters of variable strength.<sup>61</sup> Transformants were evaluated by a drop dilution growth assay on selective YNB-CSM agar plates lacking either leucine and tryptophan (-LW), leucine, tryptophan and histidine (-LWH; low stringency), leucine, tryptophan and histidine with 3-amino-1,2,4-triazole (-LWH + 3-AT, medium stringency) or leucine, tryptophan and adenine (-LWA; high stringency).

### Protein purification

pGEX-6P-3 derivatives expressing GST fusions with Knr4, Knr4<sup>ANAC</sup>, Knr4<sup>AC</sup> or Knr4<sup>ANALAC</sup> were introduced into *E. coli* BL21 (*E. coli* B; F<sup>-</sup> ompT gal dcm lon hsdS<sub>B</sub>(r<sub>B</sub>m<sub>B</sub>) [malB<sup>+</sup>]<sub>K-12</sub> ( $\lambda$ <sup>S</sup>)) for expression and purification. Bacteria were cultured at 37 °C in LB supplemented with 150 µg/mL ampicillin. Expression was induced at mid-exponential phase with 0.1 mM IPTG and continued at 24 °C for 20 hours. Bacteria from 500 mL cultures were pelleted and suspended in 30 mL of lysis buffer (10mM Tris-HCl pH 8.0, 0.1 mM EDTA, 150 mM NaCl, 5 mM DTT, 100 µg/mL lysozyme). Complete lysis was achieved by sonication. The lysate was incubated for 15 min in the presence of DNase I (100 U) and 5 mM MgSO<sub>4</sub>. After the addition of Triton X-100 (2% final), the lysate was clarified by centrifugation (22,000 g). The clear lysate was incubated for 4 h at 12 °C with 1 mL of 6B glutathione sepharose beads (GE Healthcare) equilibrated in PBS buffer (pH 7.4, 11.9 mM phosphate, 137 mM NaCl, 2.7 mM KCl). The beads were washed with PBS, and then PreScission<sup>TM</sup> protease (80 U, GE Healthcare) was added for overnight incubation in cleavage buffer (50 mM TRIS pH 7, 1 mM EDTA, 150 mM NaCl) and then used to pack an open column. Cleaved proteins were recovered in size exclusion chromatography buffer (100 mM MES, 300 mM NaCl, pH 6.0) and fractionated in the same buffer on SEC columns (HiLoad 16/60

Superdex, S75 or S200, Pharmacia). The peak protein fractions were collected and concentrated using ultracentrifugation devices (Vivaspin, Sartorius). The protein concentrations were evaluated by measuring their UV absorption at 280 nm and using theoretical molar extinction coefficients (Knr4,  $\epsilon = 60,390 \text{ M}^{-1} \cdot \text{cm}^{-1}$ ; Knr4<sup>ΔNΔC</sup>,  $\epsilon = 48,930 \text{ M}^{-1} \cdot \text{cm}^{-1}$ ; Knr4<sup>ΔC</sup>,  $\epsilon = 58,900 \text{ M}^{-1} \cdot \text{cm}^{-1}$ ; Knr4<sup>ΔNΔLΔC</sup>,  $\epsilon = 48,930 \text{ M}^{-1} \cdot \text{cm}^{-1}$ ). When necessary, proteins were stored at  $-80 \text{ }^\circ\text{C}$  after flash freezing in liquid nitrogen.

### Protein crystallization

Previously determined crystallization conditions<sup>40</sup> repeatedly yielded crystals diffracting at best to 3.5 Å resolution, which nevertheless allowed to obtain Se-SAD phases of poor quality allowing to build a partial model. The new construct described herein allowed improved purification and identification of new crystallisation conditions. Initial crystallisation conditions were identified by screening 1400 conditions using Qiagen commercial kits (Classics, AmSO4, Anions, Cations, JCSG Core I-IV, PEGs, PEG II, MPD, pHClear, pHClear II). The sitting drops were done at 285 K with the help of a crystallisation robot (NanoDrop ExtY) by mixing 200 nL of native protein (10 to 15 mg/mL) with the same volume of reservoir solution. The drops were automatically imaged with normal and UV light using an imaging robot (RockImager, RI-1000, Formulatrix). Optimisation of crystallisation conditions was performed manually using the hanging drop vapour diffusion method (2  $\mu\text{L}$ ) on siliconized glass slides and with 450  $\mu\text{L}$  reservoirs. Crystals were obtained in the presence of PEG of average molecular weight comprised between 3,000 and 6,000, at a concentration of 15 to 24 % (w/v) at a pH range of 8.0–9.0 in 100 mM bicine buffer. Seleno-methionylated protein crystallised in similar conditions, but resulted in crystals diffracting to lower resolution.

### Structure determination

Diffraction data were collected with crystals cooled in a gaseous nitrogen flux at 100 K after a brief immersion in the crystallisation solution supplemented with 20 % ethylene glycol (v/v). Native diffraction data were collected at the European Synchrotron Radiation Facility (ESRF, Grenoble, France) on beamline ID23eh1 while anomalous data were collected at ALBA (Barcelona, Spain) on beamline XALOC. Collected intensities were processed using XDS and XSCALE.<sup>62</sup> SIRAS phasing and initial model building were performed with Phenix.<sup>63</sup> Subsequent model modifications and refinement were performed with Coot,<sup>64</sup> Refmac,<sup>65</sup> and the CCP4 suite of programs.<sup>66</sup> Data processing and refinement statistics are provided [Table S4](#).

### SAXS analysis: Sample preparation and data acquisition (Details can be found in [Supplementary Table 4](#))

SAXS data were collected at the BM29 beamline (ESRF, Grenoble, France) using a Pilatus 1 M detector. The detector-distance of respectively 2.867 m covers a momentum transfer range of  $0.04 < Q < 4.94 \text{ nm}^{-1}$ . SAXS experiments were carried out at  $20 \text{ }^\circ\text{C}$  with sample concentrations ranging from 1 to 10–15  $\text{mg mL}^{-1}$  and sample volumes of 50  $\mu\text{L}$  in a quartz glass capillary, using the automated sample changer. Two mM fresh DTT was added to each sample and centrifugation was performed just before data collection. The Knr4<sup>ΔC</sup> protein, which was more sensitive to proteolysis, was investigated using the online FPLC size exclusion purification system, whereas the Knr4<sup>ΔNΔC</sup> (SD) and Knr4 proteins were batch collected. Data from the corresponding buffer (last dialysis buffer in case of batch data collection) were used to provide a reference for the scattering background. Each measurement consisted of ten frames for which radiation damage was systematically investigated.

### SAXS analysis: Data processing (Details can be found in [Supplementary Table 5](#))

Data processing was performed with the ATSAS suite of programs.<sup>57</sup> The forward scattering  $I_0$  and the radius of gyration  $R_g$  were calculated using the Guinier approximation using PRIMUS with  $Q \cdot R_g < 1.1$ , following particular recommendations for IDPs.<sup>68</sup> The calibration of the beamline was made with pure water and in such a way that  $I_0/c$  indicates the apparent molecular weight in kDa. In addition, the Rambo and Tainer concentration independent method<sup>69</sup> and the mass evaluation based on the Porod volume, as implemented in SAXSMoW<sup>70</sup> have been applied. The distance distribution function  $P(r)$  and maximum dimensions  $D_{max}$  were calculated using GNOM, which also provided a  $R_g$  calculation based on the whole scattering curve. Dimensionless Kratky plot has been calculated following the recommendations of Durand *et al.*<sup>39</sup> In the crystallographic structure 5J1B of construct Knr4<sup>ΔNΔC</sup> (SD), some residues (80–83, 149–154, 189–217, 301–309) were missing, probably due to local disorder. They have been built on an atomic resolution using AllosMod-FoXS<sup>71</sup>. Fitting of the theoretical scattering curves computed from this completed crystallographic structure with the experimental data in solution of the same construct was done using CRY SOL. More thorough analysis of the SAXS data was performed using the Ensemble Optimization Method (EOM).<sup>72–73</sup> A pool of 10,000 monomeric structures of each construct was generated with the program RanCh by connecting the crystallographic structure of the SD domain with the 80-residues and 165-residues long N-terminal and C-terminal regions (ATSAS 3.0.3 for Knr4<sup>ΔC</sup>

and Knr4, and 3.1.3 for Knr4<sup>ANΔC</sup>). The more compact option was chosen due to the partial flexibility of Knr4<sup>ΔC</sup> and Knr4. The pool of structures was submitted to the genetic algorithm (GA) to select the minimal ensemble of conformations that best reproduce the data. Various sizes of the selected subensembles were tested to check for stability as recommended in.<sup>74</sup> The results presented here are from automatic determination of the ensemble size.

### Accession numbers

All data generated or analysed during this study are included in this published article, its [supplementary information](#) files and publicly available repositories. The SAXS data have been deposited on SASBDB database (<https://www.sasbdb.org>),<sup>75</sup> under the draft identifiers SASDPC7, SASDPD7 and SASDPE7 (<https://www.sasbdb.org/data/SASDPC7/a44f0aym3x>, <https://www.sasbdb.org/data/SASDPD7/gzfijr6z6l> and <https://www.sasbdb.org/data/SASDPE7/m35nignrim>). The atomic coordinates for Knr4<sup>ANΔC</sup> and Knr4<sup>ANΔALΔC</sup> have been deposited in the Protein Data Bank (RCSB PDB, <https://www.rcsb.org>),<sup>76</sup> under the identifiers PDB ID: 5J1B (<https://doi.org/10.2210/pdb5J1B/pdb>) and PDB ID: 8AJ2 respectively.

### CRedit authorship contribution statement

**Manon Batista:** Investigation. **Ellen I.M. Donker:** Investigation. **Cécile Bon:** Investigation, Writing – original draft, Writing – review & editing. **Myriam Guillien:** Investigation. **Adriana Caisso:** Investigation. **Lionel Mourey funding:** . **Jean Marie François funding:** . **Laurent Maveyraud:** Investigation, Writing – original draft, Writing – review & editing, Supervision. **Didier Zerbib:** Conceptualization, Supervision, Writing – original draft, Writing – review & editing.

### DATA AVAILABILITY

Data will be made available on request.

### Acknowledgements

We thank the scientific staff at the European Synchrotron Radiation Facility (Grenoble, France) and ALBA (Barcelona, Spain) for the use of their excellent data collection facilities. The macromolecular crystallography equipment used in this study are part of the Integrated Screening Platform of Toulouse (PICT, IBISA). We are grateful to the Bruce Futcher's team (Stony Brook School of Medicine) for the generous gift of plasmid pGZ110. Funding was provided by the National Centre for Scientific Research (CNRS-France), the Université Paul Sabatier (Toulouse-

France) and the Institut National des Sciences Appliquées de Toulouse (INSAT-Toulouse-France).

### Declaration of Competing Interest

The authors declare that they have no known competing financial interests or personal relationships that could have appeared to influence the work reported in this paper.

### Appendix A. Supplementary data

Supplementary data to this article can be found online at <https://doi.org/10.1016/j.jmb.2023.168048>.

Received 26 October 2022;

Accepted 9 March 2023;

Available online 17 March 2023

#### Keywords:

intrinsically disordered protein;  
*Saccharomyces cerevisiae*;  
integrative structural biology;  
Knr4/Smi1;  
cell wall integrity

† These authors contributed equally to this work.

### References

- Dunker, A.K., Cortese, M.S., Romero, P., Iakoucheva, L. M., Uversky, V.N., (2005). Flexible nets. The roles of intrinsic disorder in protein interaction networks. *FEBS J.* **272**, 5129–5148.
- Oldfield, C.J., Dunker, K.A., (2014). Intrinsically Disordered Proteins and Intrinsically Disordered Protein Regions. *Annu. Rev. Biochem.* **83**, 553–584.
- Uversky, V.N., (2019). Protein intrinsic disorder and structure-function continuum. *Prog. Mol. Biol. Transl. Sci.* **166**, 1–17.
- Fung, H.Y.J., Birol, M., Rhoades, E., (2018). IDPs in macromolecular complexes: the roles of multivalent interactions in diverse assemblies. *Curr. Opin. Struct. Biol.* **49**, 36–43.
- Niklas, K.J., Dunker, A.K., Yruela, I., (2018). The evolutionary origins of cell type diversification and the role of intrinsically disordered proteins. *J. Exp. Bot.* **69**, 1437–1446.
- Yang, J., Gao, M., Xiong, J., Su, Z., Huang, Y., (2019). Features of molecular recognition of intrinsically disordered proteins via coupled folding and binding. *Protein Sci.* **28**, 1952–1965.
- Dunker, A.K., Silman, I., Uversky, V.N., Sussman, J.L., (2008). Function and structure of inherently disordered proteins. *Curr. Opin. Struct. Biol.* **18**, 756–764.
- Wright, P.E., Dyson, J.H., (2015). Intrinsically disordered proteins in cellular signalling and regulation. *Nature Rev. Mol. Cell Biol.* **16**, 18–29.
- Dosztányi, Z., Chen, J., Dunker, K.A., Simon, I., Tompa, P., (2006). Disorder and sequence repeats in hub proteins and

- their implications for network evolution. *J. Proteome Res.* **5**, 2985–2995.
10. Haynes, C., Oldfield, C.J., Ji, F., Klitgord, N., Cusick, M.E., Radivojac, P., et al., (2006). Intrinsic disorder is a common feature of hub proteins from four eukaryotic interactomes. *PLoS Comput. Biol.* **2** (8), e100.
  11. Martin-Yken, H., Francois, J.M., Zerbib, D., (2016). Knr4: A Disordered Hub Protein at the Heart of Fungal Cell Wall Signaling. *Cell. Microbiol.* **18**, 1217–1227.
  12. Wilson, D., Madera, M., Vogel, C., Chothia, C., Gough, J., (2007). The SUPERFAMILY database in 2007: families and functions. *Nucleic Acids Res.* **35**, D308–D313.
  13. Hong, Z., Mann, P., Brown, N.H., Tran, L.E., Shaw, K.J., Hare, R.S., et al., (1994). Cloning and characterization of KNR4, a yeast gene involved in (1,3)-beta-glucan synthesis. *Mol. Cell. Biol.* **14**, 1017–1025.
  14. Yamamoto, T., Uchida, K., Hiratani, T., Miyazaki, T., Yagi, J., Yamaguchi, H., (1988). In vitro activity of the killer toxin from yeast *Hansenula mrakii* against yeasts and molds. *J. Antibiot.* **41**, 398–403.
  15. Martin, H., Dagkessamanskaia, A., Satchanska, G., Dallies, N., Francois, J., (1999). KNR4, a suppressor of *Saccharomyces cerevisiae* cwh mutants, is involved in the transcriptional control of chitin synthase genes. *Microbiology* **145** (Pt 1), 249–258.
  16. Fishel, B.R., Sperry, A.O., Garrard, W.T., (1993). Yeast calmodulin and a conserved nuclear protein participate in the in vivo binding of a matrix association region. *PNAS* **90**, 5623–5627.
  17. Markovich, S., Yekutieli, A., Shalit, I., Shadkchan, Y., Oshrov, N., (2004). Genomic approach to identification of mutations affecting caspofungin susceptibility in *Saccharomyces cerevisiae*. *Antimicrob. Agents Chemother.* **48**, 3871–3876.
  18. Levin, D.E., (2005). Cell wall integrity signaling in *Saccharomyces cerevisiae*. *Microbiol Mol Biol Rev* **69**, 262–291.
  19. Cyert, M.S., (2003). Calcineurin signaling in *Saccharomyces cerevisiae*: how yeast go crazy in response to stress. *Biochem. Biophys. Res. Commun.* **311**, 1143–1150.
  20. Martin-Yken, H., Dagkessamanskaia, A., Basmaji, F., Lagorce, A., Francois, J., (2003). The interaction of Sit2 MAP kinase with Knr4 is necessary for signalling through the cell wall integrity pathway in *Saccharomyces cerevisiae*. *Mol. Microbiol.* **49**, 23–35.
  21. Heinisch, J.J., Rodicio, R., (2018). Protein kinase C in fungi—more than just cell wall integrity. *FEMS Microbiol. Rev.* **42** (1)
  22. Zhao, Y., Du, J., Zhao, G., Jiang, L., (2013). Activation of calcineurin is mainly responsible for the calcium sensitivity of gene deletion mutations in the genome of budding yeast. *Genomics* **101**, 49–56.
  23. Durand, F., Dagkessamanskaia, A., Martin-Yken, H., Graille, M., Tilbeurgh, H., Uversky, V.N., et al., (2008). Structure–function analysis of Knr4/Smi1, a newly member of intrinsically disordered proteins family, indispensable in the absence of a functional PKC1–SLT2 pathway in *Saccharomyces cerevisiae*. *Yeast* **25**, 563–576.
  24. Dagkessamanskaia, A., Durand, F., Uversky, V.N., Binda, M., Lopez, F., El Azzouzi, K., et al., (2010). Functional dissection of an intrinsically disordered protein: understanding the roles of different domains of Knr4 protein in protein-protein interactions. *Protein Sci.* **19**, 1376–1385.
  25. Costanzo, M., Baryshnikova, A., Bellay, J., Kim, Y., Spear, E.D., Sevier, C.S., et al., (2010). The genetic landscape of a cell. *Science* **327**, 425–431.
  26. Goehring, A.S., Mitchell, D.A., Tong, A.H., Keniry, M.E., Boone, C., Sprague, G.F., (2003). Synthetic lethal analysis implicates Ste20p, a p21-activated protein kinase, in polarisome activation. *Mol. Biol. Cell* **14**, 1501–1516.
  27. Lesage, G., Shapiro, J., Specht, C.A., Sdicu, A.-M.-M., Ménard, P., Hussein, S., et al., (2005). An interactional network of genes involved in chitin synthesis in *Saccharomyces cerevisiae*. *BMC Genet.* **6**, 8.
  28. Basmaji, F., Martin-Yken, H., Durand, F., Dagkessamanskaia, A., Pichereaux, C., Rossignol, M., et al., (2006). The 'interactome' of the Knr4/Smi1, a protein implicated in coordinating cell wall synthesis with bud emergence in *Saccharomyces cerevisiae*. *Molecular genetics and genomics: MGG.* **275**, 217–230.
  29. Tong, A.H., Lesage, G., Bader, G.D., Ding, H., Xu, H., Xin, X., et al., (2004). Global mapping of the yeast genetic interaction network. *Science (New York, N.Y.)* **303**, 808–813.
  30. Uetz, P., Giot, L., Cagney, G., Mansfield, T.A., Judson, R. S., Knight, J.R., et al., (2000). A comprehensive analysis of protein-protein interactions in *Saccharomyces cerevisiae*. *Nature* **403**, 623–627.
  31. Nobile, C.J., Johnson, A.D., (2015). *Candida albicans* Biofilms and Human Disease. *Annu. Rev. Microbiol.* **69**, 71–92.
  32. Martin-Yken, H., Bedekovic, T., Brand, A.C., Richard, M.L., Znaidi, S., d'Enfert, C., et al., (2018). A conserved fungal hub protein involved in adhesion and drug resistance in the human pathogen *Candida albicans*. *The Cell Surface.* **4**, 10–19.
  33. Uversky, V.N., (2013). Intrinsic disorder-based protein interactions and their modulators. *Curr. Pharm. Des.* **19**, 4191–4213.
  34. Yan, J., Dunker, A.K., Uversky, V.N., Kurgan, L., (2016). Molecular recognition features (MoRFs) in three domains of life. *Mol. Biosyst.* **12**, 697–710.
  35. Mendoza, I., Rubio, F., Rodriguez-Navarro, A., Pardo, J. M., (1994). The protein phosphatase calcineurin is essential for NaCl tolerance of *Saccharomyces cerevisiae*. *J. Biol. Chem.* **269**, 8792–8796.
  36. Rusnak, F., Mertz, P., (2000). Calcineurin: form and function. *Physiol. Rev.* **80**, 1483–1521.
  37. Van Daele, R., Spriet, I., Wauters, J., Maertens, J., Mercier, T., Van Hecke, S., et al., (2019). Antifungal drugs: What brings the future? *Med. Mycol.* **57**, S328–S343.
  38. Receveur-Brechot, V., Durand, D., (2012). How random are intrinsically disordered proteins? A small angle scattering perspective. *Curr. Protein Pept. Sci.* **13**, 55–75.
  39. Durand, D., Vives, C., Cannella, D., Perez, J., Pebay-Peyroula, E., Vachette, P., et al., (2010). NADPH oxidase activator p67(phox) behaves in solution as a multidomain protein with semi-flexible linkers. *J. Struct. Biol.* **169**, 45–53.
  40. Julien, S., Tondl, P., Durand, F., Dagkessamanskaia, A., van Tilbeurgh, H., Francois, J.M., et al., (2015). Crystallographic studies of the structured core domain of Knr4 from *Saccharomyces cerevisiae*. *Acta Crystallogr F Struct Biol Commun.* **71**, 1120–1124.
  41. Krissinel, E., Henrick, K., (2007). Inference of macromolecular assemblies from crystalline state. *J. Mol. Biol.* **372**, 774–797.

42. Murzin, A.G., Brenner, S.E., Hubbard, T., Chothia, C., (1995). SCOP: a structural classification of proteins database for the investigation of sequences and structures. *J. Mol. Biol.* **247**, 536–540.
43. Holberger, L.E., Garza-Sanchez, F., Lamoureux, J., Low, D.A., Hayes, C.S., (2012). A novel family of toxin/antitoxin proteins in *Bacillus* species. *FEBS Letter* **586**, 132–136.
44. Weinkam, P., Pons, J., Sali, A., (2012). Structure-based model of allostery predicts coupling between distant sites. *PNAS* **109**, 4875–4880.
45. Herth, W., (1980). Calcofluor white and Congo red inhibit chitin microfibril assembly of *Poteroiochromonas*: evidence for a gap between polymerization and microfibril formation. *J. Cell Biol.* **87**, 442–450.
46. Pringle, J.R., (1991). Staining of bud scars and other cell wall chitin with calcofluor. *Methods Enzymol.* **194**, 732–735.
47. Ram, A.F.J., Klis, F.M., (2006). Identification of fungal cell wall mutants using susceptibility assays based on Calcofluor white and Congo red. *Nature Protoc.* **1**, 2253–2256.
48. Roncero, C., Durán, A., (1985). Effect of Calcofluor white and Congo red on fungal cell wall morphogenesis: in vivo activation of chitin polymerization. *J. Bacteriol.* **163**, 1180–1185.
49. González-Rubio, G., Sastre-Vergara, L., Molina, M., Martín, H., Fernández-Acero, T., (2022). Substrates of the MAPK Sit2: Shaping Yeast Cell Integrity. *Journal of Fungi* **8**, 368.
50. Martin-Yken, H., Dagkessamanskaia, A., Talibi, D., Francois, J., (2002). KNR4 is a member of the PKC1 signalling pathway and genetically interacts with BCK2, a gene involved in cell cycle progression in *Saccharomyces cerevisiae*. *Curr. Genet.* **41**, 323–332.
51. Nakamura, T., Liu, Y., Hirata, D., Namba, H., Harada, S., Hirokawa, T., et al., (1993). Protein phosphatase type 2B (calcineurin)-mediated, FK506-sensitive regulation of intracellular ions in yeast is an important determinant for adaptation to high salt stress conditions. *EMBO J.* **12**, 4063–4071.
52. Dagkessamanskaia, A., El Azzouzi, K., Kikuchi, Y., Timmers, T., Ohya, Y., Francois, J.M., et al., (2010). Knr4 N-terminal domain controls its localization and function during sexual differentiation and vegetative growth. *Yeast* **27**, 563–574.
53. Hubbard, S.J., Beynon, R.J., Thornton, J.M., (1998). Assessment of conformational parameters as predictors of limited proteolytic sites in native protein structures. *Protein Eng.* **11**, 349–359.
54. Kim, D.H., Han, K.H., (2018). PreSMo Target-Binding Signatures in Intrinsically Disordered Proteins. *Mol. Cells* **41**, 889–899.
55. Bullock, B.N., Jochim, A.L., Arora, P.S., (2011). Assessing helical protein interfaces for inhibitor design. *J. Am. Chem. Soc.* **133**, 14220–14223.
56. Bah, A., Forman-Kay, J.D., (2016). Modulation of Intrinsically Disordered Protein Function by Post-translational Modifications. *J. Biol. Chem.* **291**, 6696–6705.
57. Bah, A., Vernon, R.M., Siddiqui, Z., Krzeminski, M., Muhandiram, R., Zhao, C., et al., (2015). Folding of an intrinsically disordered protein by phosphorylation as a regulatory switch. *Nature* **519**, 106–109.
58. Guillien, M., Mouhand, A., Fournet, A., Gontier, A., Marti Navia, A., Cordeiro, T.N., et al., (2022). Structural Insights into the Intrinsically Disordered GPCR C-Terminal Region, Major Actor in Arrestin-GPCR Interaction. *Biomolecules* **12** (5), 617.
59. Bous, J., Fouillen, A., Orcel, H., Trapani, S., Cong, X., Fontanel, S., et al., (2022). Structure of the vasopressin hormone-V2 receptor-beta-arrestin1 ternary complex. *Sci. Adv.* **8**, eabo7761.
60. Louvet, O., Doignon, F., Crouzet, M., (1997). Stable DNA-binding yeast vector allowing high-bait expression for use in the two-hybrid system. *Biotechniques* **23** (816–8), 20.
61. James, P., Halladay, J., Craig, E.A., (1996). Genomic libraries and a host strain designed for highly efficient two-hybrid selection in yeast. *Genetics* **144**, 1425–1436.
62. Kabsch, W., (2010). XDS. *Acta Crystallogr. D Biol. Crystallogr.* **66**, 125–132.
63. Adams, P.D., Afonine, P.V., Bunkoczi, G., Chen, V.B., Davis, I.W., Echols, N., et al., (2010). PHENIX: a comprehensive Python-based system for macromolecular structure solution. *Acta Crystallogr. D Biol. Crystallogr.* **66**, 213–221.
64. Emsley, P., Lohkamp, B., Scott, W.G., Cowtan, K., (2010). Features and development of Coot. *Acta Crystallogr. D Biol. Crystallogr.* **66**, 486–501.
65. Vagin, A.A., Steiner, R.A., Lebedev, A.A., Potterton, L., McNicholas, S., Long, F., et al., (2004). REFMAC5 dictionary: organization of prior chemical knowledge and guidelines for its use. *Acta Crystallogr. D Biol. Crystallogr.* **60**, 2184–2195.
66. Winn, M.D., Ballard, C.C., Cowtan, K.D., Dodson, E.J., Emsley, P., Evans, P.R., et al., (2011). Overview of the CCP4 suite and current developments. *Acta Crystallogr. D Biol. Crystallogr.* **67**, 235–242.
67. Franke, D., Petoukhov, M.V., Konarev, P.V., Panjkovich, A., Tuukkanen, A., Mertens, H.D.T., et al., (2017). ATSAS 2.8: a comprehensive data analysis suite for small-angle scattering from macromolecular solutions. *J. Appl. Cryst.* **50**, 1212–1225.
68. Borgia, A., Zheng, W., Buholzer, K., Borgia, M.B., Schuler, A., Hofmann, H., et al., (2016). Consistent View of Polypeptide Chain Expansion in Chemical Denaturants from Multiple Experimental Methods. *J. Am. Chem. Soc.* **138**, 11714–11726.
69. Rambo, R.P., Tainer, J.A., (2013). Accurate assessment of mass, models and resolution by small-angle scattering. *Nature* **496**, 477–481.
70. Piiadov, V., Ares de Araujo, E., Oliveira Neto, M., Craievich, A.F., Polikarpov, I., (2019). SAXSMoW 2.0: Online calculator of the molecular weight of proteins in dilute solution from experimental SAXS data measured on a relative scale. *Protein Sci.* **28**, 454–463.
71. Schneidman-Duhovny, D., Hammel, M., Tainer, J.A., Sali, A., (2016). FoXS, FoXSDock and MultiFoXS: Single-state and multi-state structural modeling of proteins and their complexes based on SAXS profiles. *Nucleic Acids Res.* **44**, W424–W429.
72. Tria, G., Mertens, H.D., Kachala, M., Svergun, D.I., (2015). Advanced ensemble modelling of flexible macromolecules using X-ray solution scattering. *IUCrJ.* **2**, 207–217.
73. Bernadó, P., Mylonas, E., Petoukhov, M.V., Blackledge, M., Svergun, D.I., (2007). Structural characterization of flexible proteins using small-angle X-ray scattering. *J. Am. Chem. Soc.* **129**, 5656–5664.
74. Sagar, A., Svergun, D., Bernado, P., (2020). Structural Analyses of Intrinsically Disordered Proteins by Small-

- Angle X-Ray Scattering. *Methods Mol. Biol.* **2141**, 249–269.
75. Kikhney, A.G., Borges, C.R., Molodenskiy, D.S., Jeffries, C.M., Svergun, D.I., (2020). SASBDB: Towards an automatically curated and validated repository for biological scattering data. *Protein Sci.* **29**, 66–75.
76. Berman, H.M., Westbrook, J., Feng, Z., Gilliland, G., Bhat, T.N., Weissig, H., et al., (2000). The Protein Data Bank. *Nucleic Acids Res.* **28**, 235–242.
77. Skolnick, J., Jaroszewski, L., Kolinski, A., Godzik, A., (1997). Derivation and testing of pair potentials for protein folding. When is the quasichemical approximation correct? *Protein Sci.* **6**, 676–688.
78. Bernado, P., Blackledge, M., (2009). A self-consistent description of the conformational behavior of chemically denatured proteins from NMR and small angle scattering. *Biophys. J.* **97**, 2839–2845.

Supplemental data

**The conserved yeast protein Knr4 involved in cell wall integrity is a multi-domain  
intrinsically disordered protein**

**Manon Batista<sup>1,2,†</sup>, Ellen I.M. Donker<sup>1,2,†</sup>, Cécile Bon<sup>2,†</sup>, Myriam Guillien<sup>1,2</sup>, Adriana Caisso<sup>1</sup>, Lionel  
Mourey<sup>2</sup>, Jean Marie François<sup>1</sup>, Laurent Maveyraud<sup>2,#</sup> and Didier Zerbib<sup>1,#</sup>**

<sup>1</sup> *Toulouse Biotechnology Institute (TBI), Université de Toulouse, CNRS, INRAE, INSA, F-31077 Toulouse, France*

<sup>2</sup> *Institut de Pharmacologie et de Biologie Structurale (IPBS), Université de Toulouse, CNRS, UPS, F-31062  
Toulouse, France*

† These authors contributed equally to this work

# Correspondence to : Didier Zerbib, *Toulouse Biotechnology Institute (TBI), Université de Toulouse, CNRS, INRAE, INSA, F-31077 Toulouse, France*, [didier.zerbib@insa-toulouse.fr](mailto:didier.zerbib@insa-toulouse.fr) , +33 (0) 561 559 966 and Laurent Maveyraud, *Institut de Pharmacologie et de Biologie Structurale (IPBS), Université de Toulouse, CNRS, UPS, F-31062 Toulouse, France*, [laurent.maveyraud@ipbs.fr](mailto:laurent.maveyraud@ipbs.fr) , +33 (0) 561 175 435.

**Supplementary Table 1** Crystallographic data processing and refinement statistics

<b>Protein</b>	<b>Knr4<sup>ΔNΔC</sup>-Se</b>	<b>Knr4<sup>ΔNΔC</sup></b>	<b>Knr4<sup>ΔNΔLΔC</sup></b>
<b>PDB ID</b>		5J1B	8AJ2
<b>Beamline</b>	ALBA, xaloc	ESRF, ID23eh1	ESRF, ID23eh1
<b>wavelength (Å)</b>	0.97949	0.972	0.972
<b>Spacegroup</b>	<i>P6<sub>2</sub></i>	<i>P6<sub>2</sub></i>	<i>P6<sub>2</sub></i>
<b>Cell parameters (Å)</b>		a=b=103.00, c=93.38	a=b=103.14, c=93.68
<b>Resolution (Å)</b>	3.20 (3.25 – 3.20)	2.50 (2.65 – 2.50)	2.20 (2.33-2.20)
<b>Number observations</b>	190,462 (7,343)	49,956 (7,939)	324,810 (52,494)
<b>Number unique</b>	18,522 (853)	19,048 (3,051)	28,788 (4,593)
<b>Multiplicity</b>	10.3 (8,6)	2.6 (2.6)	11.3 (11.4)
<b>Completeness (%)</b>	99.9 (97.4)	97.5 (97.5)	99.9 (99.7)
<b>Rsym</b>	0.174 (1.570)	0.040 (0.908)	0.071 (1.142)
<b>Rmeas</b>	0.183 (1.667)	0.054 (1.139)	0.075 (1.196)
<b>CC1/2</b>	99.7 (42.5)	99.9 (38.4)	99.9 (82.3)
<b>Anomalous correlation</b>	40	-	-
<b>SigAno</b>	1.265	-	-
<b>&lt;1/s&gt;</b>	12.98 (1.41)	12.7 (1.0)	18.7 (2.5)
<b>Resolution</b>		35.00 – 2.50	
<b>Number of reflections</b>		18,066	
<b>Rfactor/ Rfree</b>		0.1849/0.2261	
<b>Nb atoms</b>		3,417	
<b>Rms bond length (Å)</b>		0.008	
<b>Rms bond angle (°)</b>		1.132	

**Supplementary Table 2.** Essential details about SAXS data reduction, analysis and interpretation

Protein	Knr4 <sup>ΔC</sup>	Knr4 <sup>ΔNΔC</sup> (SD)	Knr4
Data reduction Software	Primusqt	Primusqt	Primusqt
Mean relative errors until 3 nm <sup>-1</sup> (%)	3.3	15.0	10.1
<b>Basic analyses</b>			
Guinier Fidelity <sup>1</sup> (%)	82	95	100
R <sub>g</sub> (nm)	2.81 ± 0.10 nm	2.29 ± 0.01 nm	4.99 ± 0.19 nm
I <sub>0</sub>	22.94 ± 0.05	27.38 ± 0.03	48.08 ± 0.06
P(r) total estimate	0.738	0.887	0.476
R <sub>g</sub> , D <sub>max</sub> (nm)	3.17 ± 0.02, 11.0 ± 0.3	2.31 ± 0.01, 8.0 ± 0.2	5.03 ± 0.01, 17.0 ± 1.0
I <sub>0</sub>	31.74 ± 0.01	27.43 ± 0.01	47.61 ± 0.05
<b>Conformational states, EOM</b>			
χ	0.93	0.68	0.88
R <sub>g</sub> (nm), D <sub>max</sub> (nm), % of population	2.5 9.1 9%	2.3 9.1 44%	3.5 10.6 7%
	2.5 9.4 36%	2.3 7.9 11%	3.6 12.0 14%
	3.1 12.3 18%	2.2 7.5 22%	3.9 15.0 7%
	3.3 11.4 9%	2.3 8.8 22%	4.1 14.3 7%
	3.4 11.7 9%		4.2 13.0 14%
	3.7 15.2 9%		4.2 13.7 7%
	4.7 18.6 9%		4.5 17.3 7%
			4.7 16.3 7%
			5.7 18.2 21%
			7.1 25.8 7%
Weighted average of R <sub>g</sub> (nm) and D <sub>max</sub> (nm)	Final ensemble: 3.1 11.6	Final ensemble: 2.3 8.5	Final ensemble: 4.6 15.6
Corresponding weighted standard deviation	0.7 2.8	0.0 0.7	1.0 3.7

**Supplementary Table 3.** Oligonucleotides used in this study

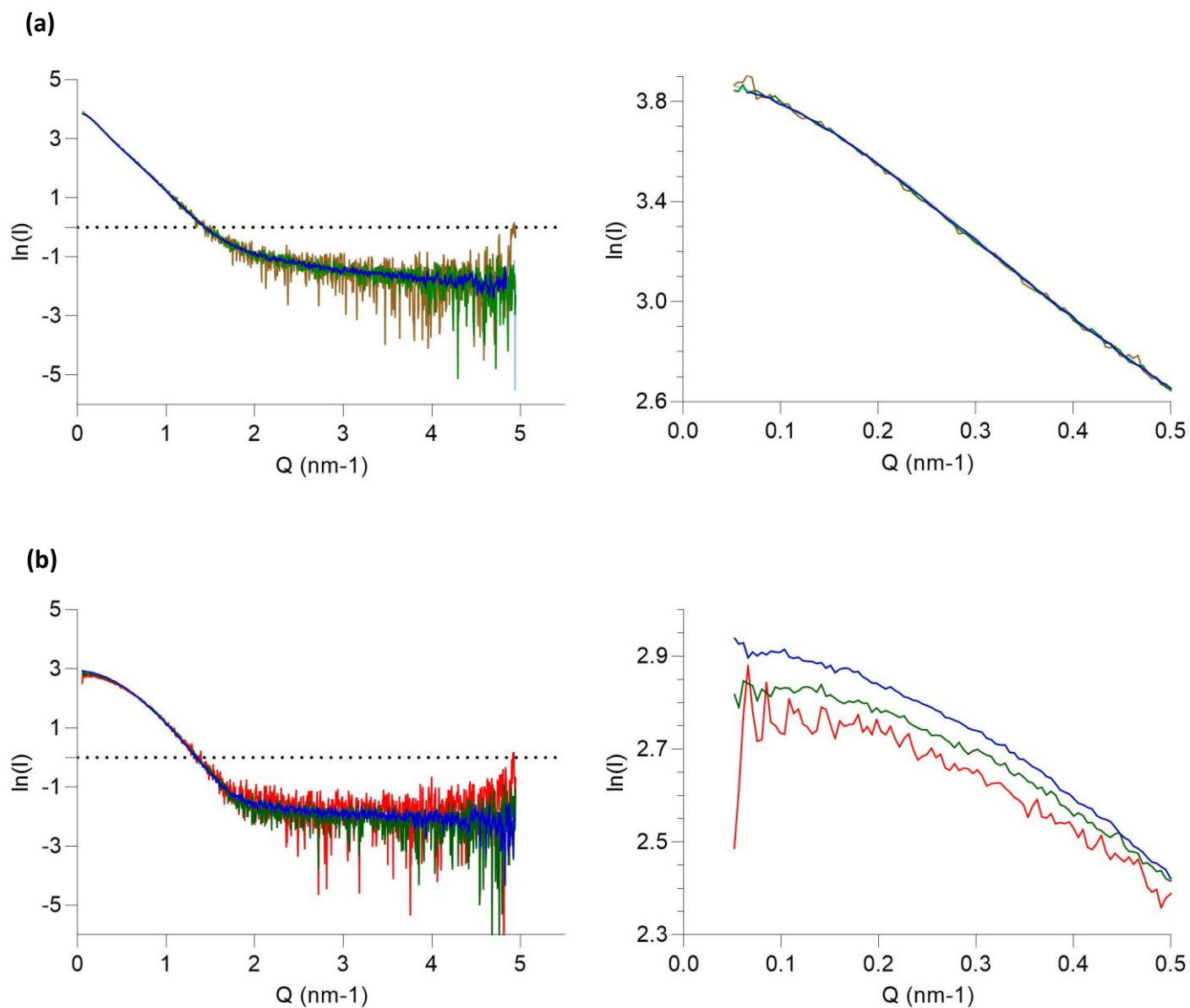
<b>Primer</b>	<b>Sequence (5' --&gt; 3')</b>	<b>Purpose</b>
<b><i>KNR4-Mut-Top</i></b>	CAAGAAACTTGAGATCTCAATAATAAAAA TCTCAACCTG	pGEX-6P-3:: Knr4 <sup>ΔC</sup> construction
<b><i>KNR4-Mut-Bot</i></b>	CAGGTTGAGATTTTTATTATTGAGATCTCAA GTTTTCTTG	pGEX-6P-3:: Knr4 <sup>ΔC</sup> construction
<b><i>KNR4-Fwd</i></b>	TACCATGGGGATCCACTAGATTTTCATCCCT	pZE13::Pro- <i>KNR4</i> -Ter construction
<b><i>KNR4-Rev</i></b>	TAAGCTTCGCGGTGGCGGC	pZE13::Pro- <i>KNR4</i> -Ter construction
<b>pZE13-Fwd</b>	GTGGATCCCATGGTACGCGTGC	pZE13::Pro- <i>KNR4</i> -Ter construction
<b>pZE13-Rev</b>	CCACCGCGAAGCTTATCGATACCGTCGACC	pZE13::Pro- <i>KNR4</i> -Ter construction
<b><i>KNR4-Rep-Fwd</i></b>	CAAGCCCTAAAGCACGTGAC	Repair Fragment
<b><i>KNR4-Rep-Rev</i></b>	CTTCGTAGTGGCCTCAAACC	Repair Fragment
<b>ΔN-Fwd</b>	TCCACGGAGTCAAACGATG	DD1 deletion in pZE13::Pro- <i>KNR4</i> -Ter
<b>ΔN-Rev</b>	CATTTTATACTAAAAATTCTGCCAAGTTG	DD1 deletion in pZE13::Pro- <i>KNR4</i> -Ter
<b>ΔL-Fwd</b>	CCAGATCAAAAATCTATTCCTCAAATG	DL deletion in pZE13::Pro- <i>KNR4</i> -Ter
<b>ΔL-Rev</b>	AGATCTTTTGTTTAGGTTCTTTGCG	DL deletion in pZE13::Pro- <i>KNR4</i> -Ter
<b>ΔC-Fwd</b>	TGAAATATCACAATTAACATTCTACAACC	DD2 deletion in pZE13::Pro- <i>KNR4</i> -Ter
<b>ΔC-Rev</b>	TTGTGATCTCAAGTTTTCTTGATACTTG	DD2 deletion in pZE13::Pro- <i>KNR4</i> -Ter

**Supplementary Table 4.** Essential details about SAXS samples

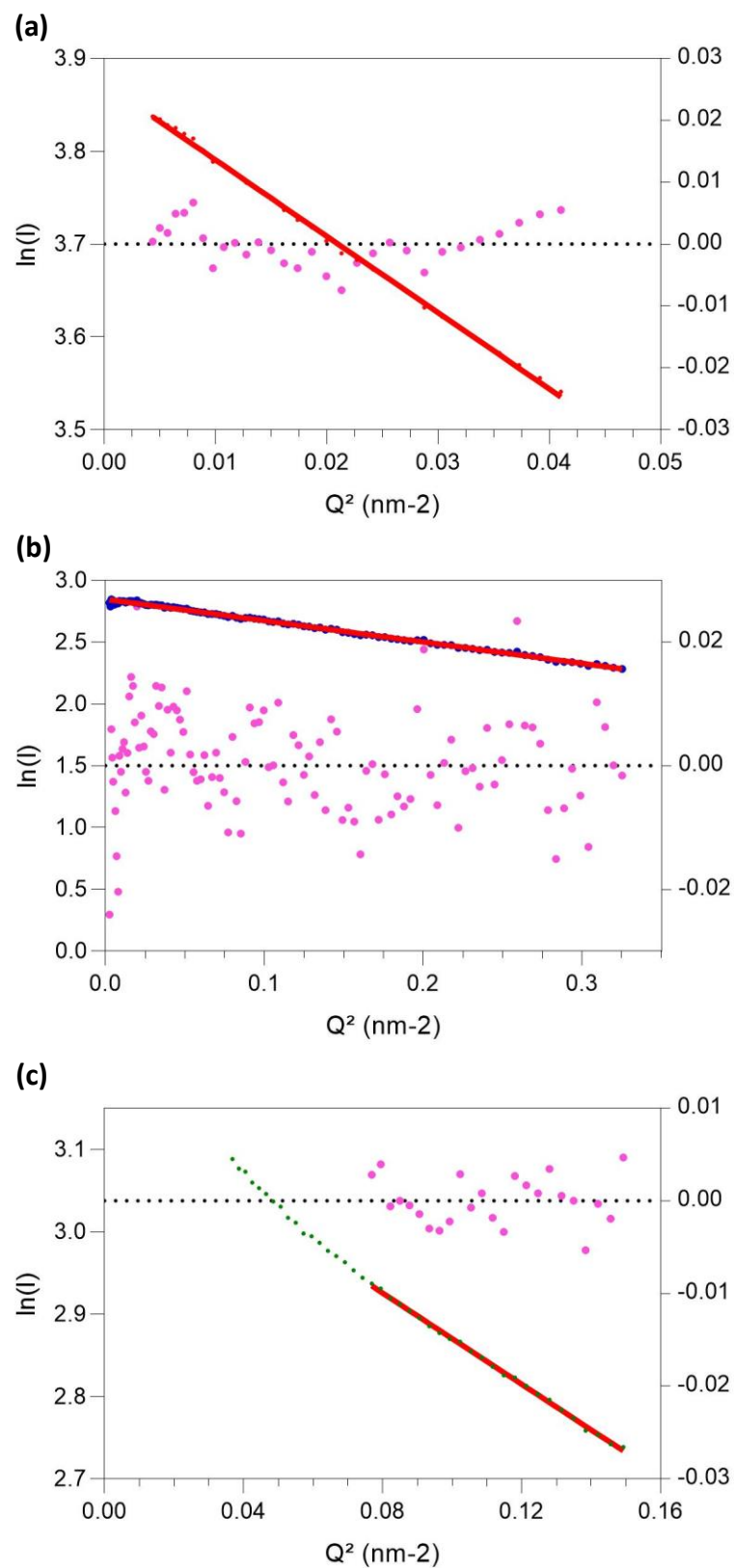
Protein	Knr4 <sup>ΔC</sup>	Knr4 <sup>ΔNΔC</sup> (SD)	Knr4
Organism	<i>Saccharomyces cerevisiae</i>		
Source	Recombinant ( <i>E. coli</i> )		
UniProt ID	P32566	P32566	P32566
Construct boundaries	1-345	80-340	1-505
N-Terminal Tag	GST, cleaved	GST, cleaved	GST, cleaved
MW (kDa)	39.6	30.9	57.5
A <sub>280nm</sub> 0.1 % (w/v)	1.586	1.488	1.050
$\bar{v}$ (cm <sup>3</sup> g <sup>-1</sup> )	0.724	0.728	0.720
$\rho_M, \rho_S, \Delta\bar{\rho}$ (all in 10 <sup>10</sup> cm <sup>-2</sup> )	12.475, 9.542, 2.933	12.420, 9.542, 2.879	12.547, 9.542, 3.006
	<b>SEC-SAXS</b>	<b>Batch-SAXS</b>	
Column	Superdex 200 5/150 GL	-	-
C <sub>load</sub> , V <sub>inject</sub>	5.5 mg.mL <sup>-1</sup> , 45 μL	-	-
Flow rate	0.3 mL.min <sup>-1</sup>	-	-
Concentration range	-	1.0-9.4 mg.mL <sup>-1</sup>	1.1-9.0 mg.mL <sup>-1</sup>
Solvent source	SEC flow-through prior to elution of protein	Last-step dialysis	Last-step dialysis

**Supplementary Table 5.** Essential details about SAXS data collection parameters acquisition

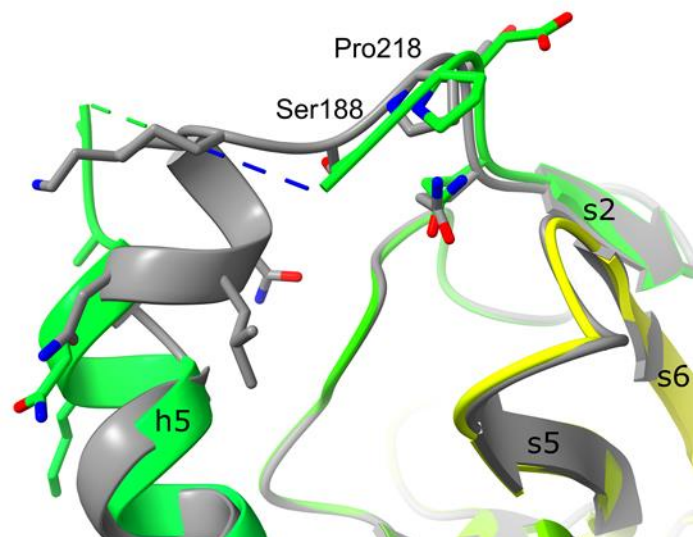
<b>Protein</b>	<b>Knr4<sup>ΔC</sup></b>	<b>Knr4<sup>ΔNΔC</sup> (SD)</b>	<b>Knr4</b>
<b>Source</b>	BM29 ESRF	BM29 ESRF	BM29 ESRF
<b>Detector</b>	Pilatus	Pilatus	Pilatus
<b>Wavelength (Å)</b>	0.9919	0.9919	0.9919
<b>Distance sample-detector (m)</b>	2.867	2.872	2.872
<b>Q-range (nm<sup>-1</sup>)</b>	0.051-4.945	0.051-4.945	0.051-4.945
<b>Temperature (°C)</b>	20.0	20.0	20.0
<b>Exposure time (s)</b>	1.5	1	1
<b>Number of frames</b>	Continuous data measurements of SEC elution	10	10
<b>Monitoring of radiation damage</b>	Frame-by-frame comparison	Frame-by-frame comparison	Frame-by-frame comparison
<b>Absolute scaling method</b>	Water calibration	Water calibration	Water calibration



**Supplementary Figure 1.** Analysis of concentration dependence for SAXS data collected in batch mode. Left, SAXS intensity normalised by concentration. Right, zoom at low  $Q$ -value. **(a).** Protein Knr4 at 1.1 mg.mL<sup>-1</sup> (brown), 2.6 mg.mL<sup>-1</sup> (green), 5.8 mg.mL<sup>-1</sup> (dark blue), 9.0 mg.mL<sup>-1</sup> (light blue). **(b).** Protein Knr4<sup>ΔNΔC</sup>(SD) at 0.97 mg.mL<sup>-1</sup> (red), 2.1 mg.mL<sup>-1</sup> (dark green), 5.7 mg.mL<sup>-1</sup> (light green), 8.08 mg.mL<sup>-1</sup> (dark blue).



**Supplementary Figure 2.** Guinier analyses of constructs. **(a).** Knr4. **(b).** Knr4<sup>AC</sup>. **(c).** Knr4<sup>ANAC</sup>.



**Supplementary Figure 3.** Superimposition of the structures of Knr4<sup>ΔNΔC</sup> (same colour as in Figure 3) and Knr4<sup>ΔNALΔC</sup> (in grey). Residues Ser188 and Pro218, that borders the deleted region in Knr4<sup>ΔNALΔC</sup> are labelled, as are the secondary structure elements.